Automated open-source software for charge transport analysis in single-carrier organic semiconductor diodes

Nikolaos Felekidis, Armantas Melianas and Martijn Kemerink

Tweet

LiU LINKÖPING UNIVERSITY

Automated open-source software for charge transport analysis in single-carrier organic semiconductor diodes

Nikolaos Felekidis[1], Armantas Melianas[2] and Martijn Kemerink[1]

[1] Complex Materials and Devices, Department of Physics, Chemistry and Biology, Linköping University, SE-581 83 Linköping, Sweden
[2] Department of Materials Science and Engineering, Stanford University, Stanford, California 94305, USA

Abstract

Organic electronics is an emerging technology with numerous applications in which the active layer is composed of an organic semiconductor (OSC) or blends of multiple OSC. One of the key performance parameters for such devices is the charge carrier mobility which can be evaluated by different measurement techniques. Here, we review different formalisms for extraction and analysis of hole mobilities from temperature-dependent space-charge limited conductivity (SCLC) measurements for pristine OSC as well as for binary and ternary blends as used in e.g. photovoltaic applications. The model is also applicable to n-type materials. Possible sources of measurement errors, such as the presence of traps and series resistance, are discussed. We show that by a simple method of selecting a proper experimental data range these errors can be avoided. The Murgatroyd-Gill analytical model in combination with the Gaussian Disorder Model is used to extract zero-field hole mobilities as well as estimates of the Gaussian energetic disorder in the HOMO level from experimental data. The resulting mobilities are in excellent agreement with those found from more elaborate fits to a full drift-diffusion model that includes a temperature, field and density dependent charge carrier mobility; the same holds for the Gaussian disorder for pure materials and blends with low fullerene concentration. The zero-field mobilities are also analyzed according to an Arrhenius model that was previously argued to reveal a universal mobility law; for most –but not all– material systems in the present work this framework gave an equally good fit to the experimental data as the other models. An automated fitting freeware, incorporating the different models, is made openly available for download and minimizes error, user input and SCLC data analysis time; e.g. SCLC current-voltage curves at several different temperatures can be globally fitted in a few seconds.

Introduction

Organic electronics is an emerging field where pristine organic semiconducting materials (OSC) as well as their blends are optimized for various applications, such as photovoltaics (OPVs),[1] light-emitting diodes (OLEDS),[2] field-effect transistors (OFETs),[3] and light-emitting electrochemical cells (LECs).[4] The performance of these light-weight, transparent, solution-processed and potentially cost-effective materials heavily relies on their charge carrier mobility. For typical OSC around room temperature the mobility is dominated by disorder and reflects the ability of the charge carriers to hop from molecular site to molecular site in a density of localized states that is broadened by energetic and spatial disorder. The charge carrier mobility μ is a valuable figure of merit to characterize the underlying physical mechanisms of charge transport as it describes the mean speed of the charge carriers under the presence of an electric field F, $v = \mu F$, and is a function of the lattice temperature as well as the charge carrier density and electric field.[5,6] Among the different experimental methods of extracting charge carrier mobilities are space-charge limited conductivity (SCLC),[7] time-of-flight (TOF),[8] dark injection,[9] Charge Carrier Extraction by Linearly Increasing Voltage (CELIV),[10,11] time-resolved Microwave Conductance (TRMC),[12] time-resolved Terahertz Spectroscopy (TRTS),[13] transient Stark spectroscopy[14] and time-resolved electric field-induced second harmonic generation (TREFISH) measurements,[15,16] each one probing different time scales following photo-excitation or charge injection and having its own limitations and advantages.

Due to its simplicity, one of the most commonly used methods is the temperature-dependent SCLC experiment that measures near-equilibrium mobilities in simple diode-type devices.[17] However, there are different empirical methods to extract charge carrier mobilities from the experimental current density vs. voltage (J-V) measurements. There are also different frameworks in which the temperature-dependence of the extracted mobilities can be interpreted. Analytical methods based on an ideal quadratic dependence of the current density on the applied bias are among the most popular and simple to use.[18,19] However, the required constant power law slope of 2 is rarely observed in actual devices, hence this method is prone to give erroneous fitted mobilities, as will be shown below. The inclusion of a phenomenological field dependence of the mobility mitigates this problem.[7,20] The resulting temperature-dependent mobilities can be analyzed according to different theories, depending on whether the extracted mobilities follow an Arrhenius ($1/T$) or a non-Arrhenius ($1/T^2$) temperature dependence.[21,22] In practice it can be hard to distinguish between these two, as will also be shown below.

Apart from the analytical models, more physical and complex approaches as drift-diffusion (DD) modeling can be used to simulate the whole device including contacts and active layer, and can reproduce steady-state experimental data using either a constant mobility or a mobility that is dependent on temperature, charge carrier density and applied field as predicted by one of the several variants of the Gaussian disorder model (GDM).[22–26] In DD, the charges are assumed to be in (quasi) thermal equilibrium with the lattice, allowing the use of (quasi) Fermi levels. Increasing further in complexity, non-equilibrium models as kinetic Monte Carlo[22,27] and 'multiple trapping and release'[28], have been shown to reproduce steady-state and transient experiments.[16,29–31] Advanced ab-initio methods, employing multi-scale modeling of the molecular morphology and electronic structure have been used to investigate the temperature-dependent mobility of both specific and generic systems.[32–35] Despite the increasing predictive power of truly or quasi atomistic models, the heavy computational demands of models beyond drift-diffusion still make those less suited for direct analysis of, and fitting to experiments. Hence, there is still a need for a more phenomenological but fast and reproducible analysis of charge transport in OCS.

In the present work we present a didactical review of the extraction and analysis of charge carrier mobilities from temperature-dependent SCLC measurements for the aforementioned analytical models as well as a Drift-Diffusion model with parametrized GDM mobilities.[7,18,19,21,22,36,37] Hence, we do not directly target new insight but try to educate and improve data analysis in the field, while also providing a lookup table for some of the materials that we have studied in our own lab. To this end, temperature-dependent SCLC experiments of pristine, binary and ternary hole-only diodes are analyzed to extract zero-field charge carrier mobilities as well as the Gaussian energetic disorder or activation energy for the HOMO level. The model can also be applied to n-type materials. The results of the analytical and numerical models are compared and the charge carrier mobilities and static Gaussian energetic disorder values extracted with different models are generally in agreement; the Gaussian disorder starts to deviate for blends with increasing fullerene concentration, most likely due to an increasing importance of long-range hops (to non-neighboring sites) that are not accounted for in the parametrized mobility functionals based on the GDM. Selection of the proper voltage range for fitting, accounting for the presence of traps and/or series resistances, is discussed. All material systems are also analyzed according to a universal Arrhenius 1/T behavior of zero-field mobilities. An automated freeware analysis tool with a graphical user interface (GUI) implementing all the different models, requiring minimal user input and processing time is openly available for download.

This work is in part an extension of that by Blakesley et al.[37] The authors of Ref. [37] propose different methods to ensure proper measurement and data analysis of unipolar SCLC devices. Discussed are amongst others the selection of proper contacts for having efficient charge injection and non-dominant series resistance, consistent device fabrication and stable electrical measurements, the identification of traps, dopants and the unipolarity of the devices, as well as the measurement and compensation of built-in fields for non-symmetric devices. In a complementary role, the present work incorporates much of this in an automated open-source tool, minimizing user input and enhancing standardization and robustness of the analysis. In addition, it adds data analysis in terms of the aforementioned different charge transport models.

Theoretical background

In this work charge transport is described at the level of drift-diffusion assuming near-equilibrium conditions with a steady-state (time-independent) mobility functional in which the effects of static diagonal, i.e. on-site, disorder are incorporated. It is not the purpose of this work to in-depth review the pros and cons of the (theoretical work underlying the) various mobility functionals that exist in literature. Instead, we give a short factual overview of the most commonly employed schemes; by incorporating these in the mentioned software tool the user can make an independent decision on which framework to use. We should stress that the open-source analysis tool can equally well be used to just extract mobilities from SCLC data that can be further analyzed in any external model.

Parametrized mobility functionals

A commonly employed mobility functional has been developed by Pasveer et al. on basis of numerical transport simulations accounting for hopping on a simple cubic lattice with uncorrelated Gaussian disorder. The authors assumed a localization length $\alpha = a_{NN}/10$ with a_{NN} the lattice constant (inter-site distance). For historical reasons this model shall here be referred to as the extended Gaussian disorder model (eGDM).[23] In particular the dependence of the zero-field mobility on the lattice temperature T and the charge carrier concentration p is given by

$$\mu(T,p) = \mu_0(T) \exp\left(\frac{1}{2}(\hat{\sigma}^2 - \hat{\sigma})(2pa_{NN}^3)^\delta\right) \quad (1)$$

where

$$\mu_0\,(T) = \mu^* c_1 \exp(-c_2 \hat{\sigma}^2) \quad (2)$$

$$\delta = 2\frac{\ln(\hat{\sigma}^2 - \hat{\sigma}) - \ln(\ln 4)}{\hat{\sigma}^2} \quad (3)$$

$$\mu^* = \frac{a^2 v_0 q}{\sigma} \quad (4)$$

$$\hat{\sigma} = \frac{\sigma}{kT} \quad (5)$$

In the above equations σ is the Gaussian energetic disorder, $\hat{\sigma}$ is the reduced disorder, v_0 is the attempt-to-hop frequency and p is the charge carrier concentration. The parametrization constants are set as c_1=0.87, c_2=0.44.[23,38] In Ref. [23] $c_1 = 1.8\times10^{-9} \approx 0.87\exp(-2a_{NN}/\alpha) = 0.87\exp(-20)$, therefore the choice c_1=0.87 implies that the (nearest neighbor) tunneling probability is assumed to be included in the anyhow poorly defined attempt-to-hop rate v_0. It is, however, important to keep in mind that mobilities in the eGDM do implicitly depend on α (through v_0) as $\mu \propto \exp(-2a_{NN}/\alpha)$, although it has been claimed otherwise.[25] The field dependence of the mobility is included via

$$\mu(T,p,E) = \mu(T,p)f(T,E) \quad (6)$$

where

$$f(T,E) = \exp\left(0.44(\hat{\sigma}^{1.5} - 2.2)\left(\sqrt{1 + 0.8E_{red}^2} - 1\right)\right) \quad (7)$$

where the reduced field is given by $E_{red} = Eqa_{NN}/\sigma$.

In addition to uncorrelated energetic disorder, the presence of molecular dipoles may give rise to spatial correlations in the energy landscape and several authors discussed how these affect especially the field dependence of the mobility.[39–41] Here, we shall employ the correlated Gaussian disorder model (cGDM) developed by Bouhassoune et al.[24] The authors used the same methodology as in the eGDM discussed above, but for an energy landscape with Gaussian disorder σ that results from randomly oriented dipole moments of equal magnitude on all lattice sites. In this case, the mobility can be described by the following phenomenological expression

$$\mu(T,p,E) = \left[\left(\mu_{low}(T,p,E)\right)^{q(\hat{\sigma})} + \left(\mu_{high}(T,p,E)\right)^{q(\hat{\sigma})}\right]^{1/q(\hat{\sigma})} \quad (8)$$

with $q(\hat{\sigma}) = 2.4/(1 - \hat{\sigma})$ and μ_{low} and μ_{high} the mobilities in the low- and high-field regimes, the parametrization of which is given in the appendix.[24]

The methodology followed to derive the above eGDM and cGDM parametrizations has been heavily criticized for giving an inadequate description of especially the field dependence of the mobility.[25,26,42] Instead, Baranovskii and coworkers argued that finite electric fields give rise to an increased effective temperature T_{eff} of the charge carrier distribution, as originally proposed by Shklovskii:[43]

$$T_{eff} = \left[T^2 + \left(\gamma \frac{qE\alpha}{k_B}\right)^2\right]^{1/2} \quad (9)$$

with $\gamma \approx 0.67$, k_B the Boltzmann constant and the localization length α acting as characteristic length scale.[25,26] In principle, Eq. 9 can be combined with 'any' model that describes the temperature dependent mobility of a hopping system, like Eq. (1) above or (19) below, by replacing T by T_{eff}. Here,

we shall combine it with the generic mobility expression for hopping on a lattice obtained from 'fat' percolation theory by Cottaar et al. and later by Nenashev et al.:[38,44]

$$\mu(T,p) = B \frac{q\omega_0}{kTa_{NN}p} \left(\frac{kT}{\sigma}\right)^{-\lambda} \exp\left(\frac{E_F(T,p) - E^*}{kT}\right) \quad (10)$$

Here, E_F and E^* are the Fermi energy and the critical energy, respectively. By comparing Eq. 10 to numerically exact simulations, Cottaar et al. showed that the latter depends weakly on the lattice and hopping model. For Miller-Abrahams hopping on a simple cubic lattice they found $E^* = -0.491\sigma$ below the center of the band. Under those conditions, the prefactor B, which is of order unity, was determined as $B = 0.47$. The tunneling frequency $\omega_0 = v_0 \exp(-2a_{NN}/\alpha)$ might, in the case of Marcus hopping, still depend on the temperature and reorganization energy.[38] For consistency with the choice $c_1 = 0.87$ above, we will replace ω_0 by v_0 in Eq. 10, i.e. include the tunneling probability in the attempt-to-hop rate. This has the added advantage that setting $\alpha = 0$ gives back the bare field-independent model Eq. 10.

There is no consensus whether the exponent λ in Eq. 10 is universal or also depends on lattice and hopping model. Since the numbers found by Cottaar vary little and are close to the universal critical exponent of the correlation length of the percolation cluster, with magnitude 0.875 ± 0.008 in the 3D case,[44] we shall use $\lambda = 0.875$. We shall refer to the combination of Eqs. 9 and 10 as the effective temperature version of the Gaussian disorder model (ET-GDM).

So far, we have addressed models in which transport takes place on a lattice, i.e. models that do not account for spatial disorder. Moreover, since a_{NN} is typically assumed to be several times larger than α, only hops to nearby sites contribute to conductivity in these models, making them effectively nearest neighbor hopping models. Clearly, most disordered organic semiconductors do show a significant level of spatial disorder as well, and it has been argued that this promotes variable range hopping (VRH) and prevents regular lattice models from giving an accurate description of the charge transport, especially at low temperatures.[25,42] However, for densely packed systems consisting of subunits with a narrow size distribution, prescribed by e.g. a molecular or monomer size, the radial distribution function will show pronounced peaks at short distances.[45,46] Hence, it is not upfront evident that at practically relevant (room) temperatures lattice models will unavoidably break down. From a more practical perspective, parametrized mobility expressions for VRH including structural disorder currently do not seem to exist. For these reasons we will limit ourselves to the mobility functions introduced above.

One-dimensional Drift-Diffusion model

Drift diffusion models rely typically on the simultaneous solution of the charge transport, continuity and Poisson equations, while contacts are accounted for as boundary conditions. The Poisson equation in one dimension is given by:

$$\nabla^2 V(x) = -\frac{\rho(x)}{\varepsilon_0 \varepsilon_r} \quad (11)$$

where V is the electrostatic potential, ρ the total charge density, ε_0 the vacuum permittivity, ε_r the material's relative dielectric constant and x is the spatial coordinate along the direction of current flow. The drift-diffusion equations for holes and electrons are:

$$j_p = -qn\mu_p p \frac{\partial}{\partial x} V - q D_p \frac{\partial}{\partial x} p \quad (12a)$$

$$j_n = -qn\mu_n \frac{\partial}{\partial x} V + q D_n \frac{\partial}{\partial x} n \quad (12b)$$

where p (n) is the hole (electron) density, $D_{p(n)}$ is the hole (electron) diffusion constant, $\mu_{p(n)}$ is the hole (electron) mobility and q is the elementary charge. The diffusion constant is assumed to be related to the mobility via the classical Einstein relation

$$\frac{D}{\mu} = \frac{k_B T}{q} \quad (13)$$

where T is the absolute temperature and μ is calculated according to equation 2. While in principle the generalized Einstein equation should be used in disordered media,[47] it has also been argued that the classical Einstein relation in disordered organic semiconductors is valid in absence of non-equilibrium effects due to e.g. deep charge traps.[48] Since we are mainly interested in the drift-dominated SCLC regime, Eq. 13 is applicable in this case.

Combining the one-dimensional drift equation, i.e. the first term in Eq. 12 with the Poisson equation under the assumption of steady-state (constant current throughout the device), one can derive the simple Mott-Gurney quadratic equation: [18,49]

$$j = \frac{9}{8} \varepsilon_0 \varepsilon_r \mu \frac{\left(V_{app} - V_{bi}\right)^2}{L^3} \quad (14)$$

where L is the device thickness, V_{app} the applied field and V_{bi} the built-in voltage.

For a general situation there is no analytical solution and one has to rely on numerical schemes to solve Eqs. (11-14). In the code used in this work, these equations are solved using the well-known Scharfetter-Gummel interpolation scheme for the free charge carrier densities and current densities; see SI for further details.[50]

Injection barriers ϕ are defined as the difference between the workfunction of the contact and the band edge (in this case the HOMO). Strictly spoken, an Ohmic contact is barrier-free. However, for the used parameters, an injection barrier between 0 eV and ~0.2 eV was found to result in a non-limiting, i.e. practically Ohmic contact. For finite-barrier contacts the image potential is included via its effect on the injection barriers as:

$$\phi' = \phi - \sqrt{\frac{q F_{int}}{4\pi \varepsilon_0 \varepsilon_r}} \quad (15)$$

provided the interfacial field F_{int} leads to a lowering of the injection barrier; otherwise the unperturbed barrier ϕ is used. The (effective) injection barrier ϕ' sets a boundary condition for the charge carrier density as:

$$p = p_0 \exp\left(-\frac{\phi'}{k_B T}\right) \quad (16)$$

where p_0 is the total site density. The effective injection barrier was not allowed to become less than zero as this would imply unphysical charge densities exceeding p_0.

Although including the effects of (energetically) discrete or distributed traps in the DD framework is relatively straightforward, it often leads to an underdetermined parameter set when fitting to actual

experiments. Hence, when one is interested in the 'intrinsic' mobility parameters, it is better to avoid the parts of the J-V curve that are trap-dominated as will be discussed in more detail below. In this work a trap-free analysis will therefore be employed for all the material systems under study. With traps, in this context, we refer to any additional distribution of localized states that sit in the bandgap and that is not included in the e.g. Gaussian density of 'free' states, even if these free states are localized too.

More details on the equations and implementation of the drift-diffusion model are found in the SI (chapter 1). Apart from the material parameters, the drift-diffusion model includes device parameters as the distance between the contacts (active layer thickness) and the energy barriers for contacts 1 and 2. In the analysis, experimentally measured thicknesses are set as constants while the contact barriers are free fitting parameters, allowed to vary between 0 eV and 0.2 eV, which is the range for an Ohmic contact.

Analytical models

The applicability of the Mott-Gurney law Eq. 14 relies on the strict quadratic dependence of the current density on the applied bias, which is easily detected as the region where the J-V curve has a slope of 2 on a double log-scale. This is rarely found in actual material systems. In particular, larger slopes can originate from energetic disorder or traps.[51,52] In order to describe this phenomenon an extended version of Eq. 14 which includes a field enhancement factor gamma (γ) was introduced by Murgatroyd and Gill (MG):[7,20]

$$J = \frac{9}{8} \varepsilon_r \varepsilon_0 \mu_0 \frac{(V - V_{bi})^2}{L^3} \exp\left(0.891\gamma \sqrt{\frac{V - V_{bi}}{L}} \right) \qquad (17)$$

where μ_0 and γ (that must be larger than or equal to 0) are the (temperature-dependent) zero-field mobilities and field enhancement factors, respectively. As in this treatment any density dependence of the mobility gets lumped into the γ parameter, μ_0 should be considered the mobility at both zero-field and zero density and as such can be compared to the corresponding parameter in GDM models. While originally derived for Coulomb traps that give rise to a detrapping rate that is proportional to $\exp(\sqrt{F})$, c.f. last term in Eq. 17, it is commonly used as a generic empirical expression. In particular, it has been observed by Gill that γ is typically linearly dependent on $1/T$ according to:[20]

$$\gamma(T) = B \left[\frac{1}{kT} - \frac{1}{kT_0} \right] \quad (18)$$

where B and T_0 are constant positive coefficients. This is, with reasonable accuracy, also the case for all materials studied in this work, as shown in Figures S1, S2 in the SI. It should be noted that in the above simple analytical model the mobility is only a function of the applied field and does not explicitly depend on the lattice temperature or the charge concentration. The T-dependence is only empirically accounted for by T-dependent μ_0 and γ, c.f. Eq. 18, and minor systematic deviations are commonly observed.

While $\gamma \geq 0$ must hold in the original Murgatroyd model, the tortuous morphology of (partially) phase separated bulk heterojunctions may give rise to a mobility that actually decreases with field.[53,54] The physical reason for this is that protrusions of one phase into the other can act as dead ends for charges being driven into them by an electric field. In Eq. 17 this can be mimicked by allowing γ to be negative. Unfortunately, this behavior closely resembles the effects of a series resistance as will be discussed below. In both cases, conventional mobility models cannot be used to interpret the data.

Intrinsic material properties as the static energetic disorder can be estimated from the interpretation of the extracted temperature-dependent mobilities. According to the Gaussian disorder model (GDM),[7,22] the zero-field mobility is described by a $1/T^2$ law:

$$\mu_0(T) = \mu^* \exp\left(-c_2\left(\frac{\sigma}{kT}\right)^2\right) \quad (19)$$

where μ^* is the mobility at infinite temperature and σ is the static Gaussian energetic disorder. In the GDM, the value of the parameter is $c_2 = (2/3)^2 \approx 0.44$.[22] The 'bare' GDM is valid in the Boltzmann limit only (low carrier density). Even though charge densities under SCLC conditions are typically low except in thin regions near the Ohmic contacts, a consistent description of SCLC transport requires accounting for the density and field dependence of the mobility also.[55–57] In particular, this is done in the various 'extended' variants of the Gaussian disorder model (eGDM, cGDM, ET-GDM) leading to the parametrized mobility functionals Eqs. 1, 8 and 10 introduced above.

An alternative approach to the GDM models discussed above is based on an Arrhenius-type analysis of the zero-field mobility dependence on temperature according to:[21]

$$\mu_0(T) = \mu^* \exp\left(-\frac{\Delta}{kT}\right) \quad (20)$$

where Δ is the activation energy. This treatment does not make any upfront assumptions about the shape of the density of states. Craciun et al. have argued that, when analyzed using Eq. 20, the SCLC J-V curves of a wide range of devices show a zero-field mobility that follows Eq. 20 with a universal mobility μ^* of 30-40 cm²/Vs.[21] On the one hand, the $1/T$-temperature dependence has been argued to result from neglecting the carrier-concentration dependence of the mobility.[57] On the other hand, recent calculations for intra-chain hopping based on a generic model Hamiltonian yielded support for a $1/T$-temperature dependence in the low-density regime.[32] In particular, it was argued that the low-field, low-density mobility depends only on two parameters, an effective structural disorder and an effective electron-phonon coupling that together determine the constants in Eq. 20. Here, we will inspect both the $1/T$- and $1/T^2$-temperature dependences by applying them to a large dataset.

The aforementioned analytical models (MG + GDM, MG + Arrhenius) as well as the drift-diffusion model with parametrized mobilities (DD + eGDM, cGDM and ET-GDM) are implemented in a freeware automated analysis tool (see SI for numerical details).[58] The DD + GDM models are expected to be more descriptive and more accurate as they explicitly solve the drift-diffusion equations and account for density and field dependencies of the mobility in a non-empirical manner, and thus serves as a proxy for the reliability of the MG + GDM model.

Experimental

Hole transport in pure, binary and ternary organic semiconductor blends as used in e.g. organic photovoltaics is investigated in the present work. More concretely, experimental temperature-dependent space-charge limited currents vs. voltage were measured for hole-only pristine TQ1, PCDTBT devices, binary blends of rr-P3HT:PC$_{61}$BM (1:1 weight ratio), PTB7:PC$_{71}$BM (1:1.5), TQ1:PC$_{71}$BM (1:2.5), APFO-Green9:PC$_{71}$BM (1:3), APFO3:PC$_{61}$BM (1:4) and MDMO:PPV:PC$_{61}$BM (1:4) as well as a series of ternary TQ1:PC$_{71}$BM$_{1-x}$:IC$_{60}$BA$_x$, (0 ≤ x ≤ 1) devices. Full names of all the compounds as well as fabrication details are given in the SI. Temperature-dependent SCLC J–Vs were measured in the dark in a Janis probe station under high vacuum (~10^{-5} mbar). The active layer thickness was determined using a Veeco Dektak 6M Stylus Profilometer. The experimental data are reproduced using an automated least-squares fitting program with a graphical user interface (GUI) that is made openly available for download and use. This analysis tool requires minimum user input as the fitting range can

be automatically detected by the software and the model fitting parameters like mobility and energetic disorder are automatically calculated.

SCLC device fabrication

Hole-only devices were fabricated according to the following process: a 40 nm thin film of poly-(3,4-ethylenedioxythiophene) polystyrene sulfonate (PEDOT:PSS) was spin-coated on pre-cleaned ITO/glass substrates in air, followed by 5 min bake on a hotplate at 120 °C. After baking, the active layer (pristine polymer and binary/ternary polymer-fullerene blends) was spin-coated in a glovebox. A 10/90 nm MoO3/Al top contact was evaporated on the active layer under high (~10^{-5} mbar) vacuum. The device areas were measured to be in the range 0.022 – 0.024 cm^2 using an optical microscope. The thicknesses of the active layers were measured to be in the range of 80 to 160 nm (Tables S3, S6 in the SI).

Results & Discussion

Identifying traps and series resistance

Robust analysis of space-charge limited transport requires the initial identification of traps and/or series resistance in the device as they must have a negligible influence to justify application of the models introduced above.[37] The presence of traps is detected by investigating the slope of the log(j)-log(V) experimental data by taking the logarithmic derivative $d(\log(j))/d(\log(V))$.[51] In general, the presence of shallow trap levels makes that only a fraction of the injected charge carriers contribute to the device current. When the trap level becomes filled a transition to a higher, trap-free SCLC current occurs. The strong dependence of the current density on the voltage in this 'trap-filling' regime will result in a distinct peak in the slope, i.e. in $d(\log(j))/d(\log(V))$.[51] An example of such a peak is shown in Figure 1a for pristine TQ1 [59] which identifies the voltage region where the trap states are being filled by the injected charge carriers. In order to ensure that the 'intrinsic' charge transport properties of the investigated material are actually probed, the fitting range has to be shifted to voltages where all the traps have been filled (trap-free regions, see Figure 1a).

It is equally important to identify any series resistance in the device which occurs typically for thinner active layers and/or at high current densities and high temperatures where the active layer resistance is small. This can also be done by investigating the power law slope of the J-V data, where the existence of a decreasing slope at higher voltages could be an indication that the current density is being limited by series resistance, e.g. as for TQ1:IC$_{60}$BA 1:1 at 300K shown in Figure 1b. An alternative explanation for the decreasing slope in the case of bulk heterojunction devices is the tortuosity of the morphology discussed above. In the present case, this is the more likely explanation since the current density in panel b of Figure 1 is actually slightly lower than in panel a, i.e. contact limitations are actually less likely to dominate. In either case, the conventional mobility models discussed here become inapplicable and the fitting voltage region of the J-V curve must be downshifted, assuring it is located before the onset of dominating series resistance (Figure 1b).

Our open-source software can automatically exclude regions with a slope below a user-defined threshold value, typically ~2 for SCLC, from the fitting. Likewise, regions where the curvature $d(slope)/dV$ is less than a user-defined minimum value, 0 in the example of Figure 1b, can be excluded automatically. We hope that using automated criteria to determine the fitting range promotes objectivity and comparability between different labs.
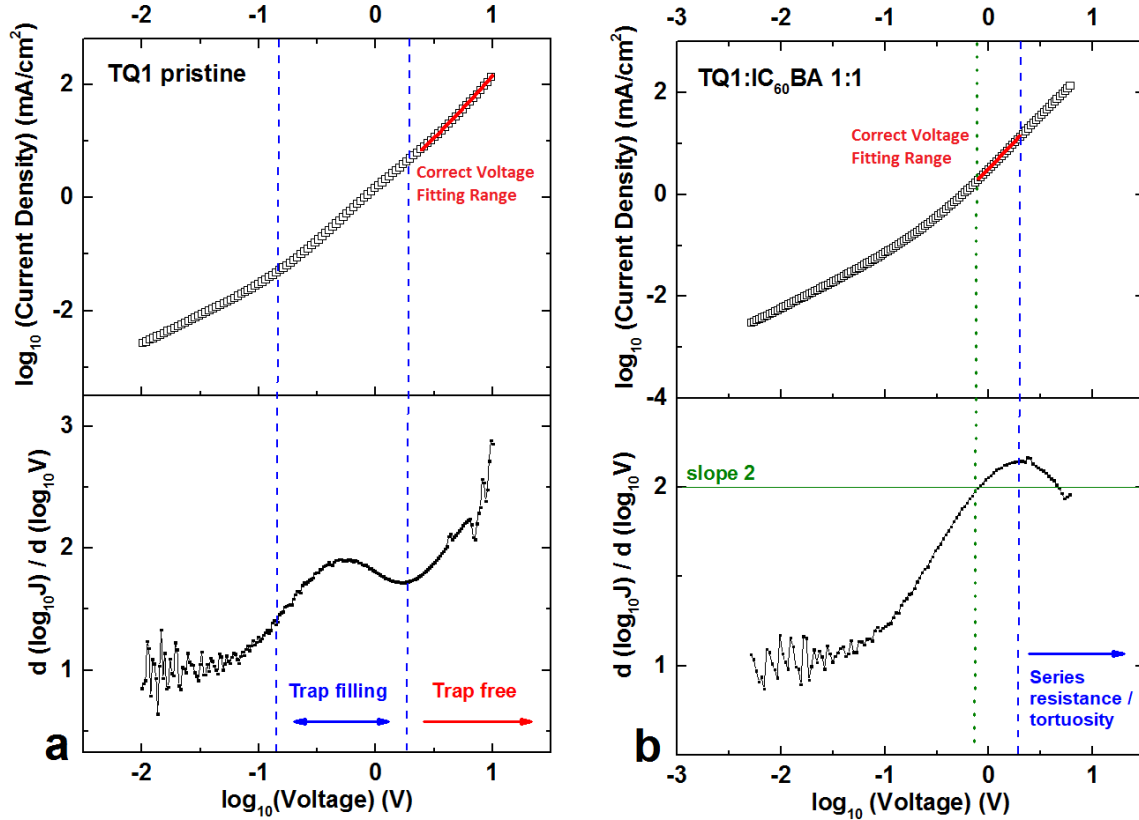
Figure 1. a) (top) SCLC data (black squares) measured at 300 K for a pristine TQ1 hole-only device, showing a peak in the slope of the double-log J-V curve as a sign of a trap-filling regime (bottom). The fitting region (red line) is confined to higher voltages where the slope is >2 and the traps are filled. b) (top) SCLC data (black squares) measured at 300 K for a binary TQ1:$IC_{60}BA$ 1:1 hole-only device showing non-negligible series resistance or tortuosity effects by a decrease in the J-V slope at higher voltages (bottom Figure). The fitting region (red line) is set at the voltage region where J-V slope >2 but before the onset where the series resistance or tortuosity dominates.

GDM analysis: Mott-Gurney vs. Murgatroyd-Gill law

Based on the Mott-Gurney law Eq. 14, the current density should be a strictly quadratic function of the applied voltage, which on a double log-scale has a slope equal to 2. Figure 2 shows two examples where this is not the case.

The Murgatroyd-Gill law Eq. 17 introduces the field-enhancement factor gamma ($\gamma \geq 0$) and allows the slope to be ≥ 2. It should be noted that the two equations are identical for $\gamma = 0$. Possibly owing to the simplicity of the model, it is not uncommon to still use Eq. 14 to fit a small voltage region of the J-V curve where the slope is equal to 2. In Figure 2 we inspect the errors that arise when different voltage regions of temperature-dependent J-V curves are fitted with Eq. 17 ($\gamma = 0$) and Eq. 17 ($\gamma > 0$), blue and red traces in Figure 2a, respectively. It is evident that the short-range fits, fitted with $\gamma = 0$, are not representative of the entire J-V curve. As such, the material is described inconsistently as different temperatures are analyzed at different field strengths.

Forcing γ to be 0 for this material system results in an overestimation of the extracted mobilities by a factor ~3-4 as seen in Figure 2b. Using the GDM model Eq. 19 to interpret the temperature-dependent mobilities results in a similar Gaussian energetic disorder estimate as mobilities at each temperature were almost equally overestimated for this specific material system. In principle, significant errors in the extracted energetic disorder should be expected as well, see e.g. the APFO3:$PC_{61}BM$ 1:4 blend for which the extracted disorders differ by 83.7meV vs 90.7meV (Figure S6). Note also that the

temperature dependence of γ obeys the empirical relation Eq. 18. In any case, to avoid errors in extracted mobility values, a common voltage range should be analyzed.
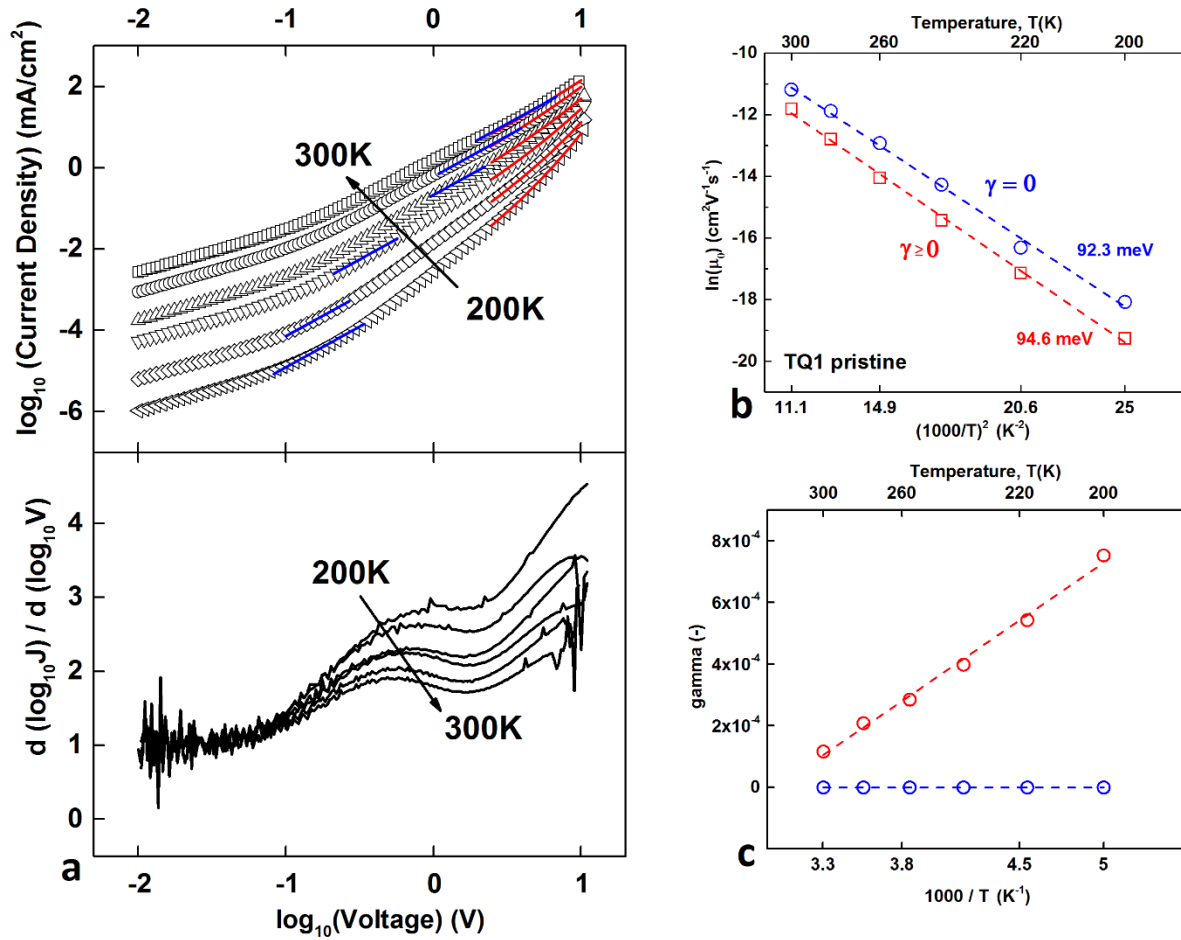
Figure 2. a) (Top) Temperature-dependent SCLC data for pristine TQ1 hole-only devices (black open symbols) fitted with Eq. 17 using γ ≥ 0 (red lines) and γ = 0 (blue lines); (bottom) the slope of the log(j)-log(V) data, showing that strict slope = 2 fitting is prone to be affected by traps; b) Extracted zero-field mobilities vs $1/T^2$ for γ ≥ 0 (red open squares) and γ = 0 (blue open circles). c) γ values and linear fits for γ > 0 and γ = 0 plotted vs $1/T$.

Mott-Gurney + GDM vs drift-diffusion + eGDM analysis in automated mode

A series of ternary $TQ1:PC_{71}BM_{1-x}:IC_{60}BA_x$, (0 ≤ x ≤ 1) hole-only devices,[52] was analyzed using the freeware analysis tool (in autorange mode, where the software automatically avoids trap-filling and series resistance problems described earlier) for both the analytical Mott-Gurney + GDM model (MG + GDM) and the drift-diffusion + eGDM (DD + eGDM) model.
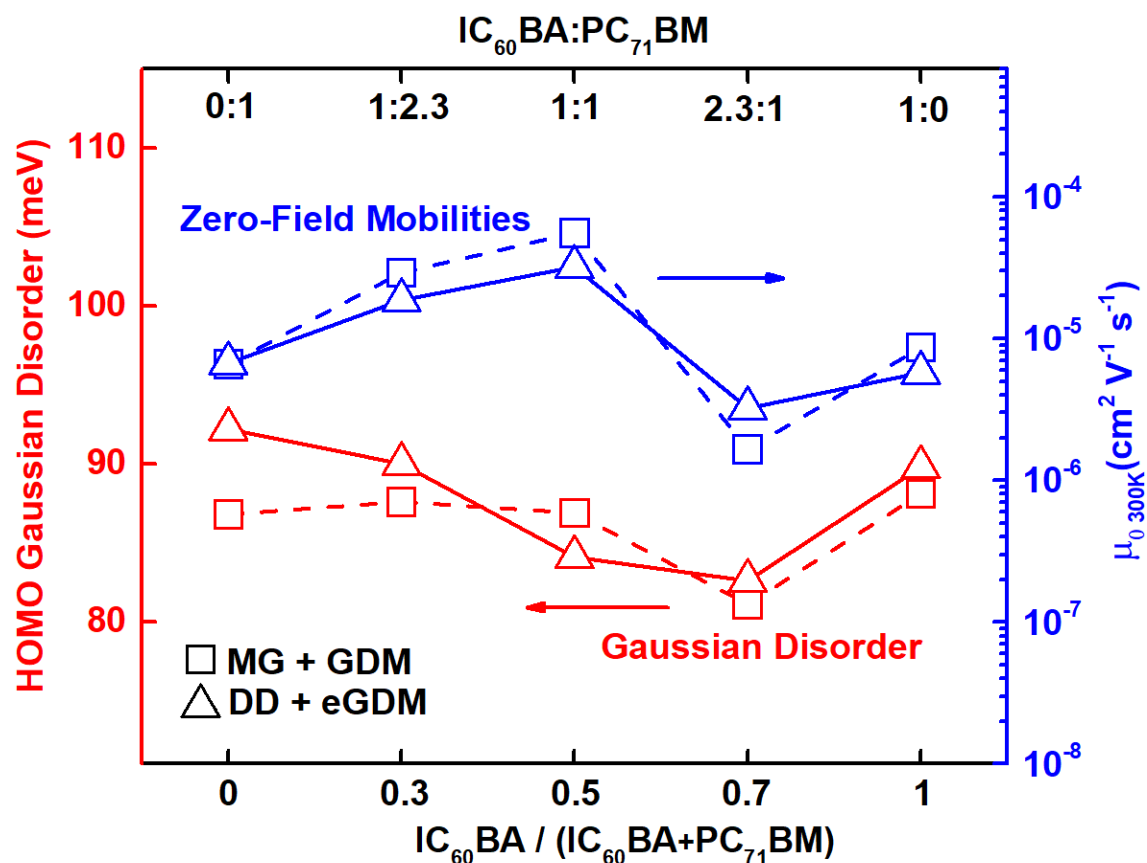
Charge carrier zero-field mobilities were calculated for DD as a function of nearest-neighbor distance, temperature, energetic disorder and hopping frequency according to the Pasveer formalism.[23] The resulting built-in voltages V_{bi} (free parameter) did not exceed 0.15V for any of the material systems studied in this work (Tables S2,S3,S5,S6 in the SI), in agreement to what has been observed experimentally, i.e. none of the devices show significant asymmetry. The resulting zero-field mobilities plotted together with the Gaussian energetic disorder estimates for the two models are shown in Figure 3; the corresponding SCLC fits are shown in Figure S1 and the fitting parameters are given in Tables S1, S2, S3.

The extracted zero-field hole mobilities (blue symbols) for the two models are in excellent agreement within a small error margin ($\pm 1 \cdot 10^{-5}$ cm^{2}V^{-1}s^{-1}). Maybe more surprisingly, in view of the differences in underlying assumptions, complexity and degrees of freedom, also the extracted Gaussian energetic disorders are in agreement within a margin of ~5 meV. In all cases, the mobility and disorder values fall well in the range of typically encountered values for this type of materials.

The MG + GDM model reproduces perfectly the experimental J-V data for all of the measured temperatures (200-300 K) and the extracted zero-field mobility and γ values follow the empirical $1/T^2$ and $1/T$ dependencies, respectively, with reasonable accuracy (SI Figures S1, S2). On the other hand, the drift-diffusion model can adequately describe the majority of the J-V curves for all of the measured temperatures (200-300K) (a reduced temperature range of 240-300K was fitted for two material systems, see SI Figures S1d, S2a). At a phenomenological level, this difference reflects the fact that the DD + eGDM model is constrained despite the larger number of parameters. At a deeper level, this reflects the fact that the eGDM model was developed for a particular mode of transport – nearest-neighbor hopping on a cubic lattice with rates described by the Miller-Abrahams expression. It was, however, shown that the mathematical form of equations 1-7 does not significantly change when other (Marcus) hopping rates or other (fcc) lattices were used,[38,60] nor when non-nearest neighbor hops and realistic, irregular site distributions are accounted for.[33] One might speculate that these models still predict a too low rate of hops to non-nearest neighbor sites and/or not fully accounting for an increased delocalization at higher energies.[32,61,62] In any case, both models predict similar energetic disorder values and can thus be used interchangeably.

Although not further pursued here, the DD + eGDM model offers the advantage over the MG + GDM model that it is not constrained to the system being in space-charge limited conditions, so sub-2 slope J-V data associated with diffusive transport can be accurately reproduced. This is shown e.g. for APFO3:PC$_{61}$BM 1:4 at 300 K in Figure S2 panel g in the SI.

The major reason for the phenomenological success of the MG + GDM model is the fact that the field enhancement factor γ, and especially its temperature-dependence, are not coupled to the disorder or any other physical parameter. Recall that, within this model, the energetic disorder is only coupled to (and extracted from) the temperature-dependence of the zero-field mobility. While phenomenologically powerful, such decoupling is unphysical. Despite this, it is an extremely convenient coincidence that the extracted mobilities and disorders from this simple analytical model are so close to those obtained with fitting with the more elaborate DD + eGDM model.

Figure 3. Zero-field charge carrier mobilities extracted from SCLC measurements performed at 300K (blue traces) and Gaussian energetic disorder (red traces) extracted using the analytical MG + GDM model (open squares) and the DD + eGDM model (open triangles) for ternary $TQ1:PC_{71}BM_{1-x}:IC_{60}BA_x$ ($0 \leq x \leq 1$) hole-only devices.

The same method as for the $TQ1:PC_{71}BM:IC_{60}BA$ system was followed to analyze a series of hole-only devices based on active layers as typically used in organic photovoltaics. The results are shown for pure materials and binary bulk heterojunction blends sorted by increasing fullerene concentration (weight fraction) in Figure 4. The SCLC fits are shown in the SI Figure S2, the corresponding parameters in Tables S4, S5 and S6. Again, the mobility and disorder values fall well in the range of typically encountered values for this type of materials.
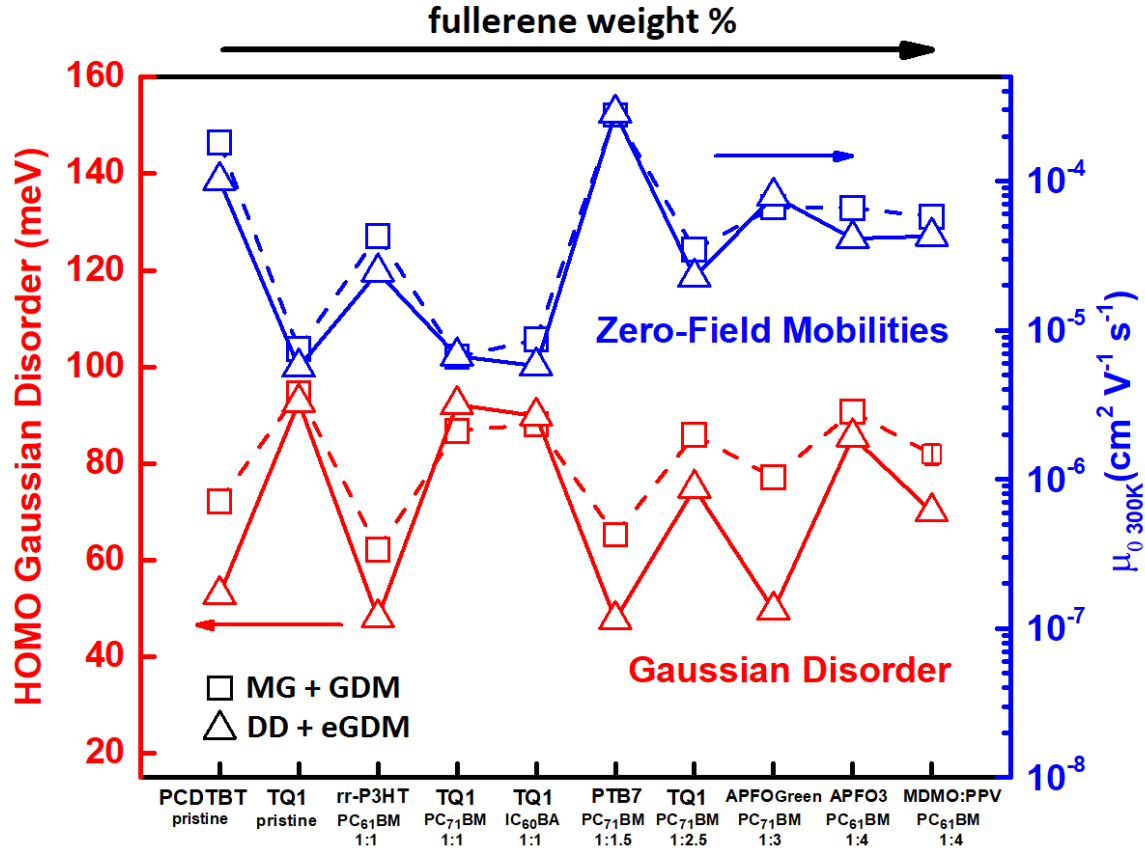
Figure 4. Charge carrier zero-field mobilities at 300K (blue traces) and Gaussian energetic disorder (red traces) extracted using the analytical MG + GDM model (open squares) and the DD + eGDM model (open triangles) for pristine, binary and ternary hole-only devices sorted by increasing fullerene concentration (weight fraction).

The resulting zero-field mobilities extracted from the J-V curves using the two models are again in agreement within a small error margin ($\pm 2 \cdot 10^{-5}$ cm^{2}V^{-1}s^{-1}). Evaluating the results from all the material systems in this work leads to the conclusion that zero-field mobility analysis within the two formalisms is in excellent agreement and therefore can empirically be trusted for both models despite the fundamental differences in underlying assumptions. However, the resulting HOMO Gaussian energetic disorders deviate by an increasing amount with increased fullerene concentration (by weight) in the blend.

At higher fullerene concentrations the Gaussian energetic disorder estimates in Figure 4 are, with one exception, significantly lower for DD + eGDM than for MG + GDM. The relatively low disorder estimates (below 60meV) for the HOMO of binary devices extracted from the DD model are not in agreement with the usual range of HOMO disorder values reported in literature (70-100meV) on basis of more elaborate analysis of multiple experiments and should therefore be considered as erroneous.[16,17,29,63] We speculate that at increasing fullerene concentrations the importance of long-range hole tunneling/hopping through the fullerene phase increases significantly as described earlier in Ref. [61], but not accounted for in eGDM-type models. Such long-range (variable range) hopping will suppress the spread of the J-V curves vs temperature. When analyzed with a model that does not account for this, the suppressed temperature dependence of the mobility will translate into an unrealistically low fitted value for the energetic disorder and should thus be avoided.

In this context it is good to discuss the general problem of parameter interchangeability when fitting transport models to J-V curves (or any multi-parameter model fit to experimental data). Within the

eGDM, the hopping rate scales the current density without changing its temperature dependence while disorder affects both, so for a single temperature measurement they are essentially indistinguishable and thereby underdetermined: the model might produce good fits, but the corresponding parameters are not unique and should not be used or trusted. For temperature-dependent measurements as done here, forcing a higher hopping rate would increase the current density resulting in a concomitant increase of the fitted energetic disorder to maintain the experimental current density. However, the induced change of energetic disorder changes the temperature-dependence and inevitably reduces the quality of the experimental SCLC data description. Hence, we cannot enforce full consistency between the DD + eGDM and GMD fit parameters by constraining the attempt-to-hop rate without the fits to the experimental data getting significantly worse. Moreover, since one has no a priori knowledge of permitted fit values in most practical situations, the hopping rate, energetic disorder and lattice constant were set as free parameters for all the material systems in this work (see SI for details). Since our model fits the entire dataset globally, the resulting fits are expected to be far less prone to errors in material parameter determination.

The fitted hopping rates and energetic disorders vary significantly among the different material systems while the inter-site distance was consistently around ~1.8 nm (arithmetic mean is ~1.7 nm) as used in previous work, [16,17,29] except for three materials systems (see SI, Table S6) where the value was ~1.3 nm (PTB7:PC$_{71}$BM 1:1.5, TQ1:PC$_{71}$BM 1:2.5, APFO3:PC$_{61}$BM 1:4). The effect of the lattice constant was found to be insignificant, and when a fixed lattice constant of 1.8 nm was enforced for the aforementioned three material systems, the resulting fits for the hopping rate and the energetic disorder were very similar without decreasing the quality of the J-V vs T fits. Accurately extracting a typical inter-site distance from temperature-dependent SCLC data using the DD + eGDM model generally requires data for devices of various thicknesses.[56,57] Based on the above and the fact that a thickness dependence study is not included in this work, we refrain from drawing firm conclusions regarding the herein obtained inter-site distances. Nevertheless, this can be incorporated into a future software release.

Mott-Gurney + GDM constrained mode

Our open-source tool offers the option of constrained GDM analysis. When activated, the field enhancement factor (γ) and zero-field mobility (μ_0) are forced to be strict functions of 1/T and 1/T^2, respectively, according to the Murgatroyd-Gill and GDM Equations 17 and 19. This mode can help to identify J-V curves that do not follow the (monotonous) trend as a function of temperature which can help to identify experimental problems during the measurement procedure. For the present material systems, constraining μ_0 and γ resulted in almost identical SCLC descriptions, i.e. identical room temperature zero-field mobilities and disorder estimates, meaning that the experimental data were sound.

Drift-diffusion + eGDM, cGDM, ET-GDM

Comparing the results of the DD+eGDM model with cGDM, the resulting disorders were found to be similar despite the J-V fits being significantly worse for all material systems when using the cGDM. Representative examples are shown in the SI (Figure S3). We conclude that for the material systems studied herein, the energetic disorder does not show correlations that are compatible with each lattice site containing a random dipole as assumed in the cGDM model. In view of the absence of significant dipole moments in most conjugated polymers, this finding is in line with expectations and previous work.[64]

The ET-GDM on the other hand can accurately reproduce the temperature-dependent J-V data over the full temperature range and yields similar disorder estimates as the eGDM; parameters and representative fits are again given in the SI (Figure S3, Table S7). Interestingly, for virtually all material systems, the fitted lattice constant and localization length are around $a_{NN} \approx 1.4$ nm and $\alpha \approx 0.25$ nm. Hence $a_{NN}/\alpha \approx$ 5-6 instead of 10 as assumed by Pasveer et al. and Bouhassoune et al. when developing the parametrizations Eqs. 1 and 8. This suggests that, from a practical perspective, varying α indeed predominantly changes the prefactor of the mobility as stated in Ref. [23]. Forcing α = 0, i.e. removing the explicit field dependence and reverting the ET-GDM to the bare Cottaar/Nenashev model Eq. 10, leads to poor fits to the J-V curves and thereby to the conclusion that not only the density dependence of the mobility must be accounted for when analyzing SCLC, as was previously argued,[55] but also – especially – its field dependence. We should finally remark that even in this α = 0 case the obtained energetic disorders are quite similar to those obtained from the complete model.

Arrhenius analysis

In earlier work a universal Arrhenius (1/T) behavior of the zero-field mobility according to equation 17 was found for a series of pristine organic semiconductors, suggesting the existence of a common infinite temperature zero-field mobility.[21] The existence of such a universal mobility would be very important as a single mobility measurement at finite temperature would suffice to characterize the full temperature dependence. The same procedure was followed here for the series of materials systems discussed above.

As a first approach the mobilities extracted from the Murgatroyd-Gill equation 17 were described by equation 20 using Δ and μ^* as free parameters. The resulting fits are plotted in Figure 5a in analogy to Ref. [21], where a strong variation of μ^* for the different materials is observed (Figure S4a). When the corresponding Δ values are plotted against μ_0 at 300K as in Ref. [21], see Figure 5b, a modest correlation is observed, with only about half of the total 13 material systems lying reasonably close to the straight dashed line. Following the method of Ref. [21] and setting a constant 'universal' μ^* = 10 $cm^2V^{-1}s^{-1}$ for all material systems gives acceptable fits for most of the material systems (9 out of 13), see Figure S3. Although the log-scaling of the plot does not allow detailed evaluation of the fit quality (Figure S3a), 4 material systems still show some deviation (Figure S5), but less than in Figure 5b. The correlation between Δ and μ_0 at 300 K evidently becomes stronger when μ^* is forced to a single value (Figure S3b). The selected universal μ^* is the arithmetic mean of the free μ^* of all the material systems μ^* = 10 $cm^2V^{-1}s^{-1}$; taking the logarithmic mean does not affect the aforementioned results/conclusions.

While the data in Figure 5 cast doubt on the validity of a strict universal Arrhenius relation between zero-field mobility and temperature as proposed in Ref. [21], the findings are in good qualitative agreement with the numerical results of Ref. [32] We should, however, point out that in the present work most materials systems are binary and ternary blends while in Refs [21,32] only pristine materials were studied. Our pristine materials TQ1 and PCDTBT fit the dependence proposed in Ref. [21].

A similar explanation could justify the fact that the universal μ^* is a factor 3 smaller than the one used in Ref. [21]. The above notwithstanding, the present experimental results do not allow to univocally point out one interpretational scheme (eGDM or Arrhenius) as superior to the other. In that perspective, it would be extremely interesting to perform layer thickness dependent studies and seek to interpret those in the Arrhenius formalism, as previously done for the DD + eGDM framework – this might for example reveal to which degree a charge carrier density dependence of the mobility, that so far has been ignored in the Arrhenius formalism, must be accounted for.
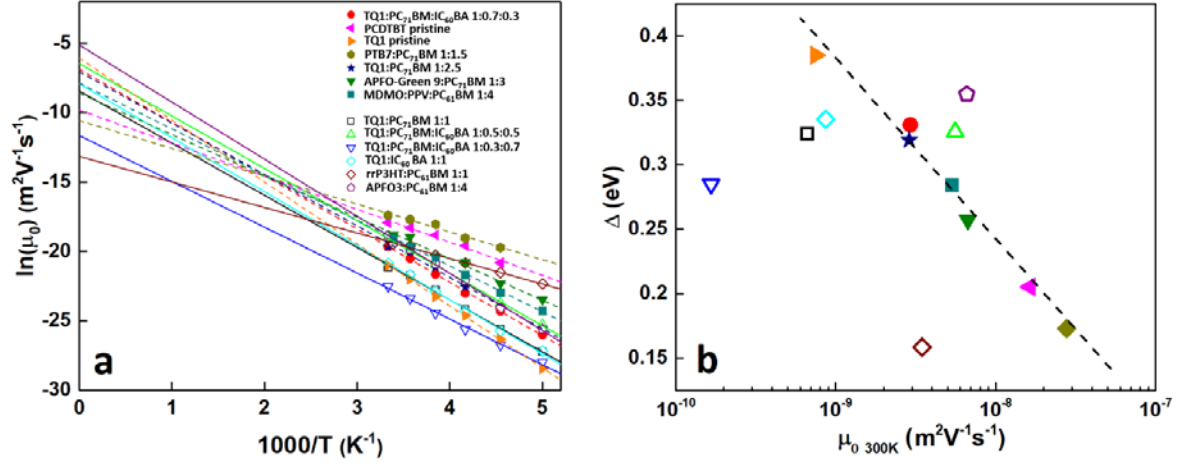
Figure 5. a) Zero-field mobilities for hole-only pristine, binary and ternary material systems fitted with equation 17 with μ^* and Δ set as free parameters. The plot is scaled as in Ref. [21] showing the resulting μ^* at infinite temperature. b) Resulting Δ values versus zero-field mobility at 300 K for all material systems. The dashed line is a guide to the eye. Solid symbols and dashed lines indicate material systems that show strong correlation between $\mu_{0\,300K}$ and Δ when μ^* is a free parameter; open symbols and solid lines indicate the material systems that do not follow the correlation trend.

Conclusion

In this work we have reviewed different equilibrium models used to extract mobilities from temperature-dependent SCLC experiments of pristine, binary and ternary hole-only devices. The Murgatroyd-Gill formalism was used to extract zero-field mobilities and was combined with the Gaussian Disorder Model in order to extract estimates of the energetic disorder. The model is also applicable to n-type materials. The above analytical model was compared to a more elaborate drift-diffusion model with parametrized mobilities according to various extensions of the Gaussian Disorder Model. Provided uncorrelated disorder is assumed, the resulting zero-field mobilities extracted with the different formalisms are in excellent agreement for all material systems while the estimated energetic disorders coincide only for those with low-fullerene concentration. The increasing deviation with increasing acceptor ratio could be attributed to the increased delocalization of the charge carriers over multiple sites while the aforementioned models are based on assumptions of nearest-neighbor hopping.

We further analyze the hole-only data assuming Arrhenius type behavior of the zero-field mobility. In previous works these were argued to follow a universal law for pristine materials. For most systems this scheme leads to an accurate description as well and we speculate that the reason for the deviation in some systems is that they are binary/ternary blends and not pure materials.

Identification of traps and series resistance is done by inspecting the slope of the log(j)-log(V) data; traps will result in a distinct peak while series resistance results in a monotonous decreasing slope at high voltages. Proper analysis of the SCLC data requires selecting an appropriate fitting voltage range which does not exhibit either of the two issues. Constraining the analysis window to the voltage where the log(j)-log(V) slope is equal to 2 results in mobilities and energetic disorder estimates that may differ considerably from the correct values. All of the aforementioned analysis models are incorporated in an automated open-source analysis tool available for download and free to use. Among other features the software provides a graphical user interface and an automated tracking of the proper voltage fitting range which reduces errors coming from user input and further increases the robustness of the analysis method while minimizing the processing time.

Acknowledgements

Appendix

For completeness, we here supply the complete parametrization of the mobility functional for the correlated Gaussian disorder model as developed by Bouhassoune et al.[24]

$$\mu(T,p,E) = \left[\left(\mu_{low}(T,p,E)\right)^{q(\hat{\sigma})} + \left(\mu_{high}(p,E)\right)^{q(\hat{\sigma})}\right]^{1/q(\hat{\sigma})}$$

For the low-density regime:

$$\mu_{low}(T,p,E) = \mu_0(T)g(T,p)f(T,E,p)$$

$$\mu_0(T) \approx \mu^* c_1 \exp(-0.29\hat{\sigma}^2)$$

where the constant $c_1 \approx 0.49\exp(-2a_{NN}/\alpha)$; as above, the exponential factor will be integrated in the hopping rate ν_0. The parametrization functions $f(T,E,p)$ and $g(T,p)$ are given by

$$g(T,p) = \exp\left((0.25\hat{\sigma}^2 + 0.7\hat{\sigma})(2pa^3)^\delta\right) \text{ for } pa_{NN}^3 < 0.025 \text{ and}$$

$$g(T,p) = g(T, 0.025a^{-3}) \text{ for } pa_{NN}^3 \geq 0.025 \text{ with}$$

$$\delta = 2.3\frac{\ln(0.5\hat{\sigma}^2 + 1.4\hat{\sigma}) - 0.327}{\hat{\sigma}^2}.$$

And

$$f(T,E_{red},p) = \exp\left(h(E_{red})\left(1.05 - 1.2(pa_{NN}^3)^{r(\hat{\sigma})}\right)\left(\hat{\sigma}^{3/2} - 2\right)\left(\sqrt{1 + 2E_{red}} - 1\right)\right)$$

with $r(\hat{\sigma}) = 0.7\hat{\sigma}^{-0.7}$. The function $h(E_{red})$ is given by

$$h(E_{red}) = \frac{4}{3}\frac{E_{red}}{E_{red}^*} \text{ for } E_{red} \leq E_{red}^*/2,$$

$$h(E_{red}) = \left[1 - \frac{4}{3}\left(\frac{E_{red}}{E_{red}^*} - 1\right)^2\right] \text{ for } E_{red}^*/2 \leq E_{red} \leq E_{red}^* \text{ and}$$

$$h(E_{red}) = 1 \text{ for } E_{red} \geq E_{red}^* \equiv 0.16.$$

As before, the reduced field equals $E_{red} = Eqa_{NN}/\sigma$

In the high-density regime:

$$\mu_{high}(p,E) = \frac{c_2}{E_{red}}\mu^*(1 - pa_{NN}^3)$$

We use $c_2 = 1$, i.e. $c_2 = \exp(-2a_{NN}/\alpha)$ in the work by Bouhassoune. Note also that the term pa_{NN}^3 equals the relative charge carrier concentration.

References

[1]   W. Zhao, D. Qian, S. Zhang, S. Li, O. Inganäs, F. Gao, J. Hou, Fullerene-Free Polymer Solar Cells with over 11% Efficiency and Excellent Thermal Stability, Adv. Mater. 28 (2016) 4734–4739. doi:10.1002/adma.201600281.

[2]   P.W.M. Blom, M.J.M. de Jong, C.T.H.F. Liedenbaum, Device physics of polymer light-emitting diodes, Polym. Adv. Technol. 9 (1998) 390–401. doi:10.1002/(SICI)1099-1581(199807)9:7<390::AID-PAT795>3.0.CO;2-9.

[3]   D. Bharti, I. Varun, S.P. Tiwari, Performance enhancement in TIPS-pentacene:PS blend organic field effect transistors by solvent vapor annealing, in: 2016 74th Annu. Device Res. Conf. DRC, IEEE, 2016: pp. 1–2. doi:10.1109/DRC.2016.7548437.

[4]   S. Tang, L. Edman, Light-Emitting Electrochemical Cells: A Review on Recent Progress, Top. Curr. Chem. 374 (2016) 40. doi:10.1007/s41061-016-0040-4.

[5]   M. Kuik, G.-J.A.H. Wetzelaer, H.T. Nicolai, N.I. Craciun, D.M. De Leeuw, P.W.M. Blom, 25th Anniversary Article: Charge Transport and Recombination in Polymer Light-Emitting Diodes, Adv. Mater. 26 (2014) 512–531. doi:10.1002/adma.201303393.

[6]   C. Tanase, E.J. Meijer, P.W.M. Blom, D.M. De Leeuw, Unification of the Hole Transport in Polymeric Field-Effect Transistors and Light-Emitting Diodes, Phys Rev Lett. (n.d.). doi:10.1103/PhysRevLett.91.216601.

[7]   P.N. Murgatroyd, Theory of space-charge-limited current enhanced by Frenkel effect, J. Phys. Appl. Phys. 3 (1970) 308. doi:10.1088/0022-3727/3/2/308.

[8]   J. Lorrmann, M. Ruf, D. Vocke, V. Dyakonov, C. Deibel, Distribution of charge carrier transport properties in organic semiconductors with Gaussian disorder, J. Appl. Phys. (2012). doi:10.1063/1.4875683.

[9]   M. Mesta, C. Schaefer, J. de Groot, J. Cottaar, R. Coehoorn, P.A. Bobbert, Charge-carrier relaxation in disordered organic semiconductors studied by dark injection: Experiment and modeling, Phys. Rev. B. 88 (2013) 174204. doi:10.1103/PhysRevB.88.174204.

[10]   G. Juška, K. Arlauskas, M. Viliūnas, J. Kočka, Extraction Current Transients: New Method of Study of Charge Transport in Microcrystalline Silicon, Phys. Rev. Lett. 84 (2000) 4946–4949. doi:10.1103/PhysRevLett.84.4946.

[11]   A.J. Mozer, G. Dennler, N.S. Sariciftci, M. Westerling, A. Pivrikas, R. Österbacka, G. Juška, Time-dependent mobility and recombination of the photoinduced charge carriers in conjugated polymer/fullerene bulk heterojunction solar cells, Phys. Rev. B. 72 (2005) 035217. doi:10.1103/PhysRevB.72.035217.

[12]   T.J. Savenije, A.J. Ferguson, N. Kopidakis, G. Rumbles, Revealing the Dynamics of Charge Carriers in Polymer:Fullerene Blends Using Photoinduced Time-Resolved Microwave Conductivity, J. Phys. Chem. C. 117 (2013) 24085–24103. doi:10.1021/jp406706u.

[13]   C.S. Ponseca, H. Němec, N. Vukmirović, S. Fusco, E. Wang, M.R. Andersson, P. Chabera, A. Yartsev, V. Sundström, Electron and Hole Contributions to the Terahertz Photoconductivity of a Conjugated Polymer:Fullerene Blend Identified, J. Phys. Chem. Lett. 3 (2012) 2442–2446. doi:10.1021/jz301013u.

[14]   J. Cabanillas-Gonzalez, T. Virgili, A. Gambetta, G. Lanzani, T.D. Anthopoulos, D.M. de Leeuw, Photoinduced Transient Stark Spectroscopy in Organic Semiconductors: A Method for Charge Mobility Determination in the Picosecond Regime, Phys. Rev. Lett. 96 (2006) 106601. doi:10.1103/PhysRevLett.96.106601.

[15]   A. Devižis, K. Meerholz, D. Hertel, V. Gulbinas, Hierarchical charge carrier motion in conjugated polymers, Chem. Phys. Lett. 498 (2010) 302–306. doi:10.1016/j.cplett.2010.08.071.

[16]   A. Melianas, V. Pranculis, A. Devižis, V. Gulbinas, O. Inganäs, M. Kemerink, Dispersion-Dominated Photocurrent in Polymer:Fullerene Solar Cells, Adv. Funct. Mater. 24 (2014) 4507–4514. doi:10.1002/adfm.201400404.

[17] A. Melianas, V. Pranculis, Y. Xia, N. Felekidis, O. Inganäs, V. Gulbinas, M. Kemerink, Photogenerated Carrier Mobility Significantly Exceeds Injected Carrier Mobility in Organic Solar Cells, Adv. Energy Mater. (2017) 1602143. doi:10.1002/aenm.201602143.

[18] M.A. Lampert, R.B. Schilling, Current Injection in Solids: The Regional Approximation Method, Semicond. Semimet. (n.d.). http://download.xuebalib.com/xuebalib.com.17303.pdf.

[19] P.W.M. Blom, M.C.J.M. Vissenberg, Charge transport in poly(p-phenylene vinylene) light-emitting diodes, Mater. Sci. Eng. R Rep. (n.d.). doi:10.1016/S0927-796X(00)00009-7.

[20] W.D. Gill, Drift mobilities in amorphous charge-transfer complexes of trinitrofluorenone and poly-n-vinylcarbazole, J. Appl. Phys. 43 (1972) 5033–5040. doi:10.1063/1.1661065.

[21] N.I. Craciun, J. Wildeman, P.W.M. Blom, Universal Arrhenius Temperature Activated Charge Transport in Diodes from Disordered Organic Semiconductors, Phys. Rev. Lett. 100 (2008) 056601. doi:10.1103/PhysRevLett.100.056601.

[22] H. Bässler, Charge Transport in Disordered Organic Photoconductors a Monte Carlo Simulation Study, Phys. Status Solidi B. 175 (1993) 15–56. doi:10.1002/pssb.2221750102.

[23] W.F. Pasveer, J. Cottaar, C. Tanase, R. Coehoorn, P.A. Bobbert, P.W.M. Blom, D.M. De Leeuw, M.A.J. Michels, Unified Description of Charge-Carrier Mobilities in Disordered Semiconducting Polymers, Phys Rev Lett. (n.d.). doi:10.1103/PhysRevLett.94.206601.

[24] M. Bouhassoune, S.L.M. van Mensfoort, P.A. Bobbert, R. Coehoorn, Carrier-density and field-dependent charge-carrier mobility in organic semiconductors with correlated Gaussian disorder, Org. Electron. 10 (2009) 437–445. doi:10.1016/J.ORGEL.2009.01.005.

[25] J.O. Oelerich, A.V. Nenashev, A.V. Dvurechenskii, F. Gebhard, S.D. Baranovskii, Field dependence of hopping mobility: Lattice models against spatial disorder, Phys. Rev. B. 96 (1952). doi:10.1103/PhysRevB.96.195208.

[26] A.V. Nenashev, J.O. Oelerich, A.V. Dvurechenskii, F. Gebhard, S.D. Baranovskii, Fundamental characteristic length scale for the field dependence of hopping charge transport in disordered organic semiconductors, Phys. Rev. B. 96 (2017). doi:10.1103/PhysRevB.96.035204.

[27] R. Volpi, S. Stafström, M. Linares, Transition fields in organic materials: From percolation to inverted Marcus regime. A consistent Monte Carlo simulation in disordered PPV, J. Chem. Phys. 142 (2015) 094503. doi:10.1063/1.4913733.

[28] J. Noolandi, Equivalence of multiple-trapping model and time-dependent random walk, Phys. Rev. B. 16 (1977) 4474–4479. doi:10.1103/PhysRevB.16.4474.

[29] N. Felekidis, A. Melianas, M. Kemerink, Nonequilibrium drift-diffusion model for organic semiconductor devices, Phys. Rev. B. 94 (2016) 035205. doi:10.1103/PhysRevB.94.035205.

[30] R.C.I. MacKenzie, A. Göritz, S. Greedy, E. von Hauff, J. Nelson, Theory of Stark spectroscopy transients from thin film organic semiconducting devices, Phys. Rev. B. 89 (2014) 195307. doi:10.1103/PhysRevB.89.195307.

[31] H. Mäckel, R.C.I. MacKenzie, Determination of Charge-Carrier Mobility in Disordered Thin-Film Solar Cells as a Function of Current Density, Phys. Rev. Appl. 9 (2018) 034020. doi:10.1103/PhysRevApplied.9.034020.

[32] R.P. Fornari, P.W.M. Blom, A. Troisi, How Many Parameters Actually Affect the Mobility of Conjugated Polymers?, Phys. Rev. Lett. 118 (2017) 086601. doi:10.1103/PhysRevLett.118.086601.

[33] A. Massé, P. Friederich, F. Symalla, F. Liu, V. Meded, R. Coehoorn, W. Wenzel, P.A. Bobbert, Effects of energy correlations and superexchange on charge transport and exciton formation in amorphous molecular semiconductors: An ab initio study, Phys. Rev. B. 95 (2017) 115204. doi:10.1103/PhysRevB.95.115204.

[34] F. Symalla, P. Friederich, A. Massé, V. Meded, R. Coehoorn, P. Bobbert, W. Wenzel, Charge Transport by Superexchange in Molecular Host-Guest Systems, Phys. Rev. Lett. 117 (2016) 276803. doi:10.1103/PhysRevLett.117.276803.

[35] L. Sousa, R. Volpi, D.A. da Silva Filho, M. Linares, Mobility field and mobility temperature dependence in PC61BM: A kinetic Monte-Carlo study, Chem. Phys. Lett. 689 (2017) 74–81. doi:10.1016/J.CPLETT.2017.10.011.

[36] J.C. Blakesley, H.S. Clubb, N.C. Greenham, Temperature-dependent electron and hole transport in disordered semiconducting polymers: Analysis of energetic disorder, Phys Rev B. (n.d.). doi:10.1103/PhysRevB.81.045210.

[37] J.C. Blakesley, F.A. Castro, W. Kylberg, G.F.A. Dibb, C. Arantes, R. Valaski, M. Cremona, J.S. Kim, J.-S. Kim, Towards reliable charge-mobility benchmark measurements for organic semiconductors, Org. Electron. 15 (2014) 1263–1272. doi:10.1016/J.ORGEL.2014.02.008.

[38] J. Cottaar, L.J.A. Koster, R. Coehoorn, P.A. Bobbert, Scaling Theory for Percolative Charge Transport in Disordered Molecular Semiconductors, Phys. Rev. Lett. 107 (2011) 136601. doi:10.1103/PhysRevLett.107.136601.

[39] Y.N. Gartstein, E.M. Conwell, High-field hopping mobility in molecular systems with spatially correlated energetic disorder, Chem. Phys. Lett. 245 (1995) 351–358. doi:10.1016/0009-2614(95)01031-4.

[40] D.H. Dunlap, P.E. Parris, V.M. Kenkre, Charge-Dipole Model for the Universal Field Dependence of Mobilities in Molecularly Doped Polymers, Phys. Rev. Lett. 77 (1996) 542–545. doi:10.1103/PhysRevLett.77.542.

[41] S.V. Novikov, D.H. Dunlap, V.M. Kenkre, P.E. Parris, A.V. Vannikov, Essential Role of Correlations in Governing Charge Transport in Disordered Organic Materials, Phys. Rev. Lett. 81 (1998) 4472–4475. doi:10.1103/PhysRevLett.81.4472.

[42] P. Kumar, V. Rani, al -, A.V. Nenashev, J.O. Oelerich, S.D. Baranovskii, Theoretical tools for the description of charge transport in disordered organic semiconductors, J. Phys. Condens. Matter. 27 (2015) 093201. doi:10.1088/0953-8984/27/9/093201.

[43] S. Marianer, B.I. Shklovskii, Effective temperature of hopping electrons in a strong electric field, Phys. Rev. B. 46 (1992). https://journals.aps.org/prb/pdf/10.1103/PhysRevB.46.13100.

[44] A.V. Nenashev, F. Jansson, J.O. Oelerich, D. Huemmer, A.V. Dvurechenskii, F. Gebhard, S.D. Baranovskii, Advanced percolation solution for hopping conductivity, Phys. Rev. B. 87 (2013) 235204. doi:10.1103/PhysRevB.87.235204.

[45] P. Kordt, J.J.M. van der Holst, M. Al Helwi, W. Kowalsky, F. May, A. Badinski, C. Lennartz, D. Andrienko, Modeling of Organic Light Emitting Diodes: From Molecular to Device Properties, Adv. Funct. Mater. 25 (2015) 1955–1971. doi:10.1002/adfm.201403004.

[46] R. Volpi, S. Kottravel, M.S. Nørby, S. Stafström, M. Linares, Effect of Polarization on the Mobility of C60: A Kinetic Monte Carlo Study, J. Chem. Theory Comput. 12 (2016) 812–824. doi:10.1021/acs.jctc.5b00975.

[47] Y. Roichman, N. Tessler, Generalized Einstein relation for disordered semiconductors—implications for device performance, Appl. Phys. Lett. 80 (2002) 1948–1950. doi:10.1063/1.1461419.

[48] G.A.H. Wetzelaer, L.J.A. Koster, P.W.M. Blom, Validity of the Einstein Relation in Disordered Organic Semiconductors, Phys. Rev. Lett. 107 (2011) 066605. doi:10.1103/PhysRevLett.107.066605.

[49] P.A. Leighton, Electronic Processes in Ionic Crystals (Mott, N. F.; Gurney, R. W.), J. Chem. Educ. 18 (1941) 249. doi:10.1021/ed018p249.1.

[50] D.L. Scharfetter, H.K. Gummel, Large-signal analysis of a silicon Read diode oscillator, IEEE Trans. Electron Devices. 16 (1969) 64–77. doi:10.1109/T-ED.1969.16566.

[51] G. Zuo, Z. Li, O. Andersson, H. Abdalla, E. Wang, M. Kemerink, Molecular Doping and Trap Filling in Organic Semiconductor Host–Guest Systems, J. Phys. Chem. C. (2017) acs.jpcc.7b01758. doi:10.1021/acs.jpcc.7b01758.

[52] N. Felekidis, A. Melianas, M. Kemerink, Design Rule for Improved Open-Circuit Voltage in Binary and Ternary Organic Solar Cells, ACS Appl. Mater. Interfaces. 9 (2017). doi:10.1021/acsami.7b08276.

[53] M.C. Heiber, K. Kister, A. Baumann, V. Dyakonov, C. Deibel, T.-Q. Nguyen, Impact of Tortuosity on Charge-Carrier Transport in Organic Bulk Heterojunction Blends, Phys. Rev. Appl. 8 (2017) 054043. doi:10.1103/PhysRevApplied.8.054043.

[54] L.J.A. Koster, Charge carrier mobility in disordered organic blends for photovoltaics, Phys. Rev. B. 81 (2010) 205318. doi:10.1103/PhysRevB.81.205318.

[55] P.W.M. Blom, C. Tanase, D.M. de Leeuw, R. Coehoorn, Thickness scaling of the space-charge-limited current in poly(p-phenylene vinylene), Appl. Phys. Lett. 86 (2005) 092105. doi:10.1063/1.1868865.

[56] S.L.M. van Mensfoort, R. Coehoorn, Effect of Gaussian disorder on the voltage dependence of the current density in sandwich-type devices based on organic semiconductors, Phys. Rev. B. 78 (2008) 085207. doi:10.1103/PhysRevB.78.085207.

[57] S.L.M. van Mensfoort, S.I.E. Vulto, R.A.J. Janssen, R. Coehoorn, Hole transport in polyfluorene-based sandwich-type devices: Quantitative analysis of the role of energetic disorder, Phys. Rev. B. 78 (2008) 085208. doi:10.1103/PhysRevB.78.085208.

[58] M.Kemerink, FitSCLC, 2018. https://github.com/mkemerink/FitSCLC.

[59] E. Wang, J. Bergqvist, K. Vandewal, Z. Ma, L. Hou, A. Lundin, S. Himmelberger, A. Salleo, C. Müller, O. Inganäs, F. Zhang, M.R. Andersson, Conformational Disorder Enhances Solubility and Photovoltaic Performance of a Thiophene-Quinoxaline Copolymer, Adv. Energy Mater. 3 (2013) 806–814. doi:10.1002/aenm.201201019.

[60] J. Cottaar, R. Coehoorn, P.A. Bobbert, Scaling theory for percolative charge transport in molecular semiconductors: Correlated versus uncorrelated energetic disorder, Phys. Rev. B. 85 (2012) 245205. doi:10.1103/PhysRevB.85.245205.

[61] A. Melianas, V. Pranculis, D. Spoltore, J. Benduhn, O. Inganäs, V. Gulbinas, K. Vandewal, M. Kemerink, Charge Transport in Pure and Mixed Phases in Organic Solar Cells, Adv. Energy Mater. (2017) 1700888. doi:10.1002/aenm.201700888.

[62] H. Abdalla, G. Zuo, M. Kemerink, Range and energetics of charge hopping in organic semiconductors, Phys. Rev. B. 96 (2017) 241202. doi:10.1103/PhysRevB.96.241202.

[63] H. van Eersel, R.A.J. Janssen, M. Kemerink, Mechanism for Efficient Photoinduced Charge Separation at Disordered Organic Heterointerfaces, Adv. Funct. Mater. 22 (2012) 2700–2708. doi:10.1002/adfm.201200249.

[64] R.J. de Vries, S.L.M. van Mensfoort, V. Shabro, S.I.E. Vulto, R.A.J. Janssen, R. Coehoorn, Analysis of hole transport in a polyfluorene-based copolymer— evidence for the absence of correlated disorder, Appl. Phys. Lett. 94 (2009) 163307. doi:10.1063/1.3119317.

Supporting Info

Automated open-source software for charge transport analysis in single-carrier organic semiconductor diodes

Nikolaos Felekidis[1], Armantas Melianas[2] and Martijn Kemerink[1]

[1] Complex Materials and Devices, Department of Physics, Chemistry and Biology, Linköping University, SE-581 83 Linköping, Sweden
[2] Department of Materials Science and Engineering, Stanford University, Stanford, California 94305, USA

Contents

1

1 - One dimensional drift diffusion model complementary equations

Equation 11 in the main text is solved using the discretization:

$$\frac{1}{h^2}(V_{i+1} + V_{i-1} - 2V_i) = -\frac{\rho_i}{\varepsilon_0\varepsilon_r} \quad (1)$$

where h is the mesh spacing, V the electrostatic potential, ρ the total charge density, ε_0 the vacuum permittivity and ε_r the dielectric constant. This results in a $N \times N$ tridiagonal matrix $\bar{\bar{P}}$, having on the first and last row only a '1' as entry on the diagonal, to account for the boundary conditions for V as set by the contacts. Using $\bar{\bar{P}}\bar{V} = -\frac{h^2}{\varepsilon_0\varepsilon_r}\bar{R}$ where $\bar{V}$ is a column vector containing V_i and $\bar{R}$ a column vector containing ρ_i except the first and last entries which are equal to the electrostatic potential of the left and right contact, respectively. Equation 12 in the main text results in hole currents:

$$j_{i+\frac{1}{2}} = -\frac{q\mu_p}{h}(V_{i+1} - V_i)\left(\frac{p_i}{1 - \exp\left(\Delta E_{i+\frac{1}{2}}\right)} + \frac{p_{i+1}}{1 - \exp\left(-\Delta E_{i+\frac{1}{2}}\right)}\right) \quad (2)$$

With, in the normal Scharfetter-Gummel scheme, $\Delta E_{i+\frac{1}{2}} = \frac{V_{i+1} - V_i}{k_B T}$.[1] For brevity, the subscripts in $\mu_{i+\frac{1}{2}}$ are dropped. Note also that the term between brackets is the interpolated hole density $p_{i+1/2}$, i.e. $j_{i+\frac{1}{2}} = -q\mu p_{i+1/2}F_{i+1/2}$ (Ohm's law) where the field $F_{i+1/2} = \frac{V_{i+1} - V_i}{h}$ is constant between mesh points. It should be noted that $p_{i+1/2}$ is not a real density and may be negative in cases diffusion dominates over drift! In order to allow use of the generalized Einstein equation we use $\Delta E_{i+1/2} = \frac{v_{i+1/2}h}{D} = \frac{\mu}{D}(V_{i+1} - V_i)$ as $v = \mu\frac{V_{i+1} - V_i}{h}$ and $D = \mu k_B T$.[2,3] This gives:

$$j_{i+\frac{1}{2}} = -\frac{qD}{h}\left(\frac{\frac{\mu}{D}(V_{i+1} - V_i)p_i}{1 - \exp\left(\frac{\mu}{D}(V_{i+1} - V_i)\right)} + \frac{\frac{\mu}{D}(V_{i+1} - V_i)p_{i+1}}{1 - \exp\left(-\frac{\mu}{D}(V_{i+1} - V_i)\right)}\right) \quad (3)$$

Using the Bernoulli function $B(x) = \frac{x}{1 - \exp(x)} = \frac{x}{2}\left(1 - \frac{1}{\tanh\left(\frac{x}{2}\right)}\right)$ this can be written as

$$j_{i+1/2} = -\frac{qD}{h}\left(B\left(Y_{i+\frac{1}{2}}\right)p_i - B\left(-Y_{i+\frac{1}{2}}\right)p_{i+1}\right) \quad (4)$$

with $Y_{i+1/2} = \frac{\mu}{D}(V_{i+1} - V_i)$. The second guise of the Bernoulli function is preferred for numerical evaluation around $x = 0$. Moreover, using the identity $\frac{x}{\tanh(-x)} = \frac{-x}{\tanh(x)}$, $\tanh()$ has to be evaluated only once.

Taking the limit of zero electric field using $B(0) = -1$ it is derived that $j_{i+\frac{1}{2}} = -\frac{qD}{h}(p_{i-1} - p_i)$ which is the common discretization of the diffusion equation for holes, $j_{p,diff} = -qD\frac{\partial p}{\partial x}$. Likewise, taking the limit of dominant drift, $|\mu(V_{i+1} - V_i)| \gg D$, the upwind discretization of the drift equation for holes is obtained, $j_{p,drift} = -q\mu\frac{(V_{i+1} - V_i)}{h}p_{i+1}$ for $(V_{i+1} - V_i) > 0$ and $j_{p,drift} = -q\mu\frac{(V_{i+1} - V_i)}{h}p_i$ for $(V_{i+1} - V_i) < 0$.

For electrons, the current density becomes

2

$$j_{i+1/2} = -\frac{q\mu}{h}(V_{i+1} - V_i)\left(\frac{n_i}{1 - \exp\left(-\Delta E_{i+\frac{1}{2}}\right)} + \frac{n_{i+1}}{1 - \exp\left(\Delta E_{i+\frac{1}{2}}\right)}\right) \quad (5)$$

$$j_{i+1/2} = -\frac{qD}{h}\left(\frac{\frac{\mu}{D}(V_{i+1} - V_i)n_i}{1 - \exp\left(-\frac{\mu}{D}(V_{i+1} - V_i)\right)} + \frac{\frac{\mu}{D}(V_{i+1} - V_i)n_{i+1}}{1 - \exp\left(\frac{\mu}{D}(V_{i+1} - V_i)\right)}\right) \quad (6)$$

$$j_{i+\frac{1}{2}} = -\frac{qD}{h}\left(-B\left(-Y_{i+\frac{1}{2}}\right)n_i + B\left(Y_{i+\frac{1}{2}}\right)n_{i+1}\right) \quad (7)$$

Using the continuity equation in steady state

$$\frac{\partial}{\partial x}j_p = q(G - R) \quad (8)$$

$$\frac{\partial}{\partial x}j_n = -q(G - R) \quad (9)$$

it is derived for holes

$$\frac{j_{i+1/2} - j_{i-1/2}}{h} = q(G_i - R_i) = qU_i \quad (10)$$

and for electrons

$$\frac{j_{i+1/2} - j_{i-1/2}}{h} = -q(G_i - R_i) = -qU_i \quad (11)$$

For equations 11 and 12 above, they can be cast as an $N \times N$ tridiagonal matrix, similarly to the Poisson equation, having only a '1' on the first and last row as entry on the diagonal to account for the boundary conditions for p and n, respectively, as set by the contacts. For holes one has $\bar{\bar{C}}\bar{P} = qh\bar{U}$ with $\bar{P}$ a column vector containing p_i and $\bar{U}$ a column vector containing U_i except at the 1st and Nth entries that are equal to the densities at the left and right contact, respectively.

2 - Derivation of equation 17 in main text

SCLC zero field mobilities (μ_0) and gamma (γ) values were extracted from the Murgatroyd-Gill law following the equation:[4,5]

$$J = \frac{9}{8}\varepsilon_r\varepsilon_0\mu_0\frac{(V - V_{bi})^2}{L^3} \cdot e^{\left(0.891\gamma\sqrt{\frac{V - V_{bi}}{L}}\right)} \quad (12)$$

where

$$\gamma(T) = \left(\frac{e^3}{\pi\varepsilon\varepsilon_0}\right)^{\frac{1}{2}}\left[\frac{1}{kT}ln\frac{N_c}{N_t} - \frac{1}{(kT)^2}E_{trap}\right] \quad (13)$$
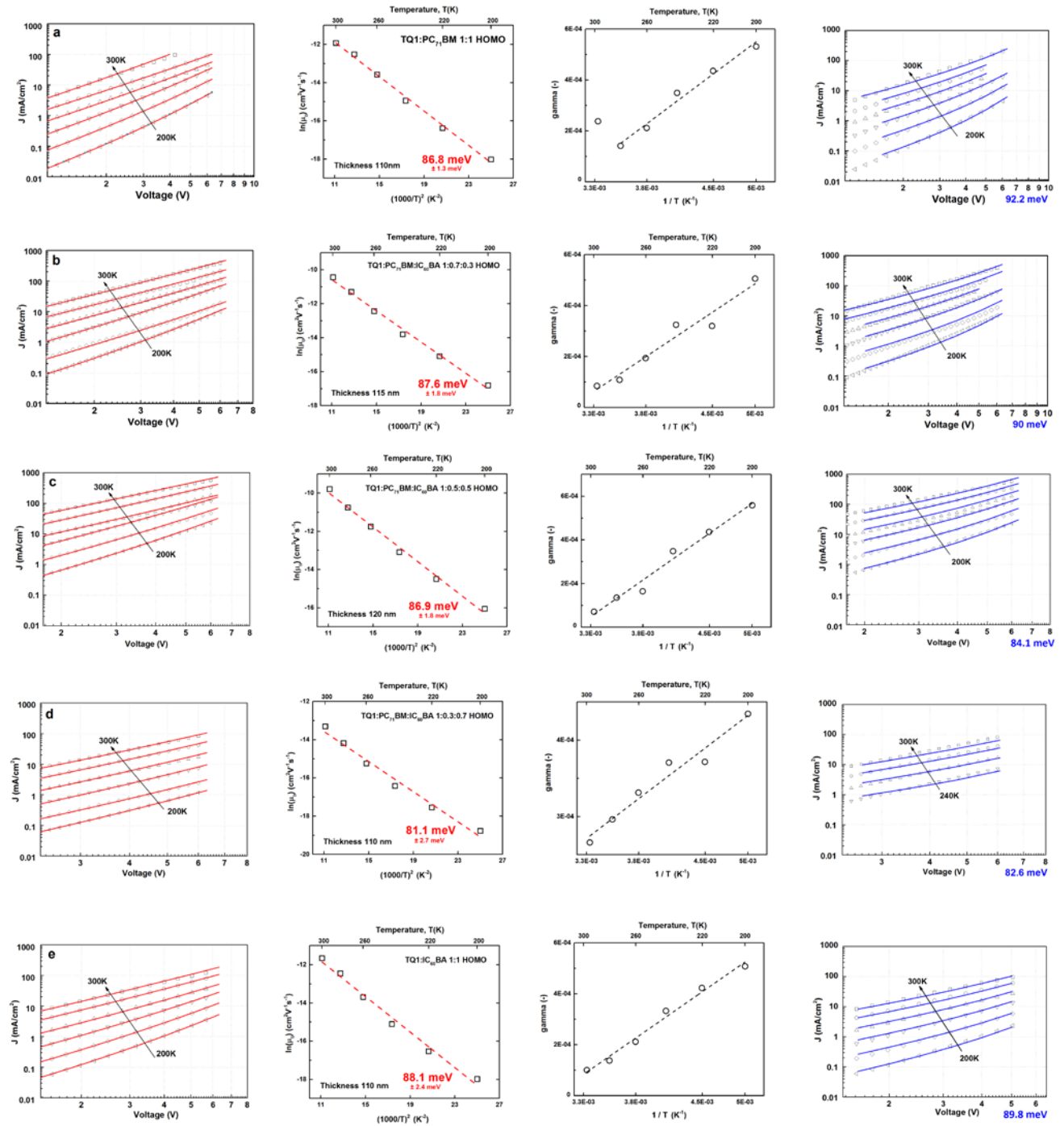
which can be obtained following the derivation by Murgatroyd in Ref. [4] using:

$$J = \frac{9}{8}\mu\epsilon\epsilon_0\frac{V^2}{L^3}\theta_0 e^{\left(\frac{0.891}{kT}\left(\frac{e^3 V}{\pi\varepsilon\varepsilon_0 L}\right)^{\frac{1}{2}}\right)} \quad (14)$$

$$\theta_0 = \frac{N_c}{N_t}e^{\left(-\frac{E_{trap}}{kT}\right)} \quad (15)$$

3

In the above equations ε_0 is the vacuum permittivity, ε_r is the dielectric constant of the material, V is the applied voltage, V_{bi} is the built-in field of the device, μ_0 is the zero field mobility, γ is the field enhancement factor, L is the distance between the electrodes, N_c is the effective density of states, N_t is the density of traps, k is the Boltzmann constant, T is the temperature, e the elementary charge, E_{trap} refers to a single trap situated at energy E_{trap} below the conduction band edge and θ_0 describes the fraction of free charges.

Figure S1. (Left) Hole-only SCLC TQ1:PC$_{71}$BM$_{1-x}$:IC$_{60}$BA$_x$ (0 ≤ x ≤ 1) data fitted with the Murgatroyd-Gill law.[4,5](Middle-left) Gaussian disorder model fit and active layer thickness. (Middle-right) Linear fit of the gamma values according to equation 17 in the main text. (Right) SCLC data fitted with the DD+eGDM model.

4 - Gaussian disorder and room temperature zero-field mobilities for MG+GDM and DD+eGDM models of the ternary TQ1:PC$_{71}$BM:IC$_{60}$BA hole-only devices shown in Figure 3

	MG+GDM		DD+eGDM	
	σ_{HOMO} [meV]	μ_0 (300 K) [cm^{2}V^{-1}s^{-1}]	σ_{HOMO} [meV]	μ_0 (300 K) [cm^{2}V^{-1}s^{-1}]
TQ1:PC$_{71}$BM 1:1	86.8	6.62·10^{-6}	92.2	6.71·10^{-6}
TQ1:PC$_{71}$BM:IC$_{60}$BA 1:0.7:0.3	87.6	2.92·10^{-5}	90	1.87·10^{-5}
TQ1:PC$_{71}$BM:IC$_{60}$BA 1:0.5:0.5	86.9	5.57·10^{-5}	84.1	3.2·10^{-5}
TQ1:PC$_{71}$BM:IC$_{60}$BA 1:0.3:0.7	81.1	1.66·10^{-6}	82.6[*]	3.23·10^{-6}
TQ1:IC$_{60}$BA 1:1	88.1	8.66·10^{-6}	89.8	5.76·10^{-6}

Table S1. Gaussian energetic disorder and room temperature zero-field mobilities for TQ1:PC$_{71}$BM$_{1-x}$:IC$_{60}$BA$_x$ (0 ≤ x ≤ 1) hole-only devices from the MG+GDM and DD+eGDM models. [*]The hopping rate and lattice constant were fixed for TQ1:PC$_{71}$BM:IC$_{60}$BA 1:0.3:0.7 (see Table S3) while 4 temperatures (240K – 300K) were fitted.

All fits were done using the auto-range mode of the SCLC fitting program. The fitting settings for GDM are: nMin=10, Vmin=0.2 V, slope min=1.7, slope target=2, curve min=0, initial guesses: μ^*= 1e-7 cm^{2}V^{-1}s^{-1} (±3 orders of magnitude), σ=75 meV (limits 25-200 meV), B=2.8·10^{-5}(±3 orders of magnitude), T$_0$=600 K (limits 1-3000 K), $\phi_{1,2}$ = 0.1 (± 0.2 V). The minor difference in Gaussian energetic disorders compared to Ref. [6] is due to the different voltage ranges used for fitting the temperature-dependent JV curves. In Ref. [6] the fitting ranges were set manually and slightly differed among the different JVs while in this case the auto-range mode resulted in a single voltage range for all the JV curves.

For the DD+eGDM model the settings of the fitting program were: nMin=10, Vmin=2 V, slope Min = 1.7, slope target = 2, curve min = -0.5. Initial guesses were: σ=75 meV (± 50 meV), hopping rate 1e9 s^{-1} (±2 orders of magnitude), $\phi_{1,2}$ = 0.1 eV (± 0.2 meV) and a$_{NN}$=1.2 nm (limits 1 nm – 4 nm). Speed mode was enabled for faster calculations. Thickness was fixed to the experimentally measured value for all material systems. Different initial guess values introduced insignificant variations in the resulting fitting parameters. The rest of the settings were left to the default values.

5 - Fitting parameters of MG+GDM model of Figure 3

	V_{bi}	μ^*	B	T_0	Error JV
	[V]	[m²V⁻¹s⁻¹]	[-]	[K]	[-]
TQ1:PC$_{71}$BM 1:1	0.0055	$9.85 \cdot 10^{-8}$	$1.9 \cdot 10^{-5}$	379.6	0.00644
TQ1:PC$_{71}$BM:IC$_{60}$BA 1:0.7:0.3	0.0185	$3.96 \cdot 10^{-7}$	$2.14 \cdot 10^{-5}$	328.2	0.00624
TQ1:PC$_{71}$BM:IC$_{60}$BA 1:0.5:0.5	0.0176	$6.72 \cdot 10^{-7}$	$2.62 \cdot 10^{-5}$	318.6	0.00631
TQ1:PC$_{71}$BM:IC$_{60}$BA 1:0.3:0.7	0.0257	$9.76 \cdot 10^{-9}$	$8.15 \cdot 10^{-6}$	2319	0.00955
TQ1:IC$_{60}$BA 1:1	-0.0320	$1.23 \cdot 10^{-7}$	$2.23 \cdot 10^{-5}$	336.2	0.00213

Table S2. Fitting parameters for TQ1:PC$_{71}$BM$_{1-x}$:IC$_{60}$BA$_x$ (0 ≤ x ≤ 1) hole-only devices extracted from the MG+GDM model.
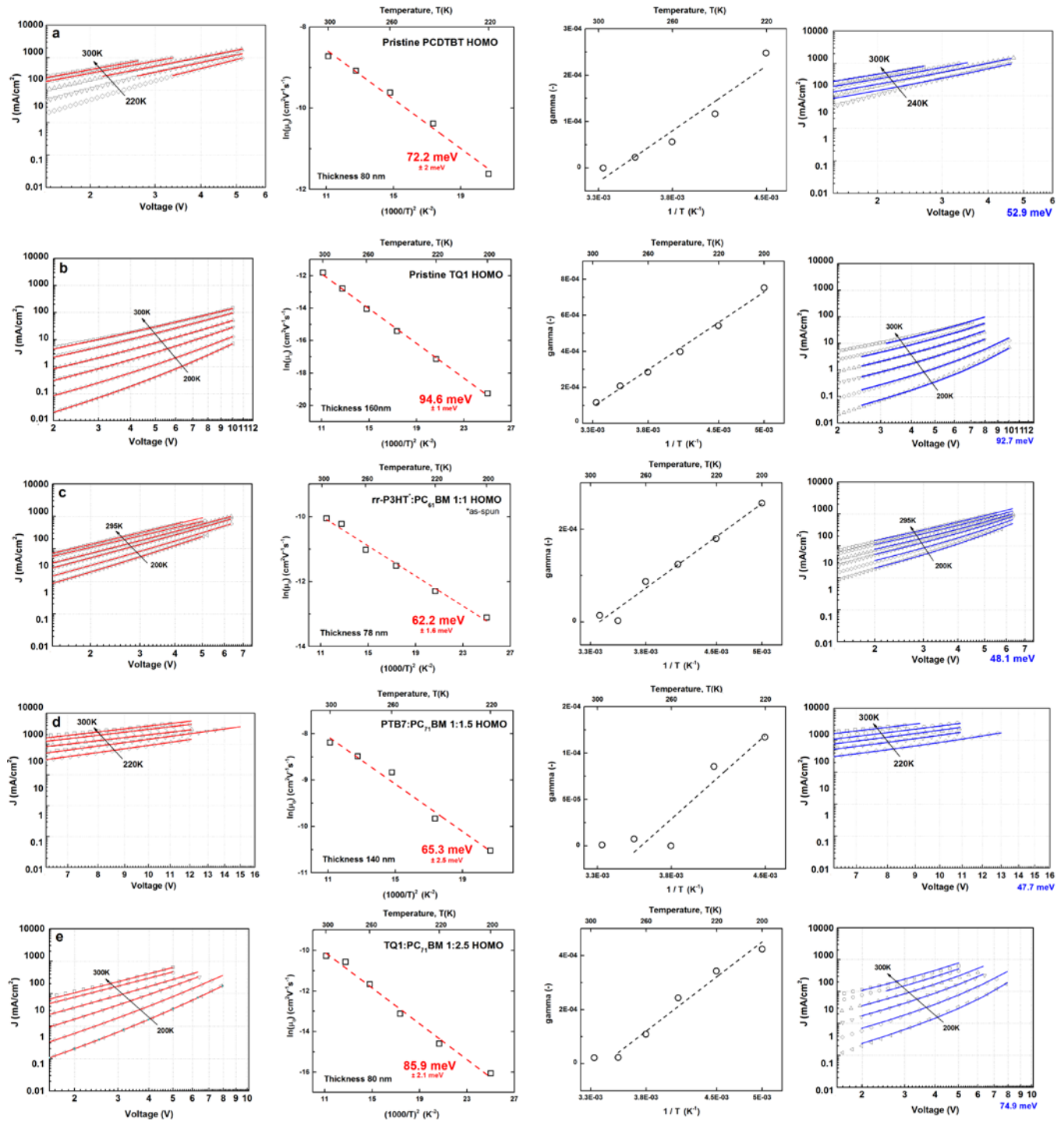
The Error JV is the one returned from the least squares fitting algorithm and refers to the deviation of the fitted curves to all the experimental datasets. The outlying fitting parameters for the TQ1:PC$_{71}$BM:IC$_{60}$BA 1:0.3:0.7 system originate from the very low measured current densities vs. applied voltage.
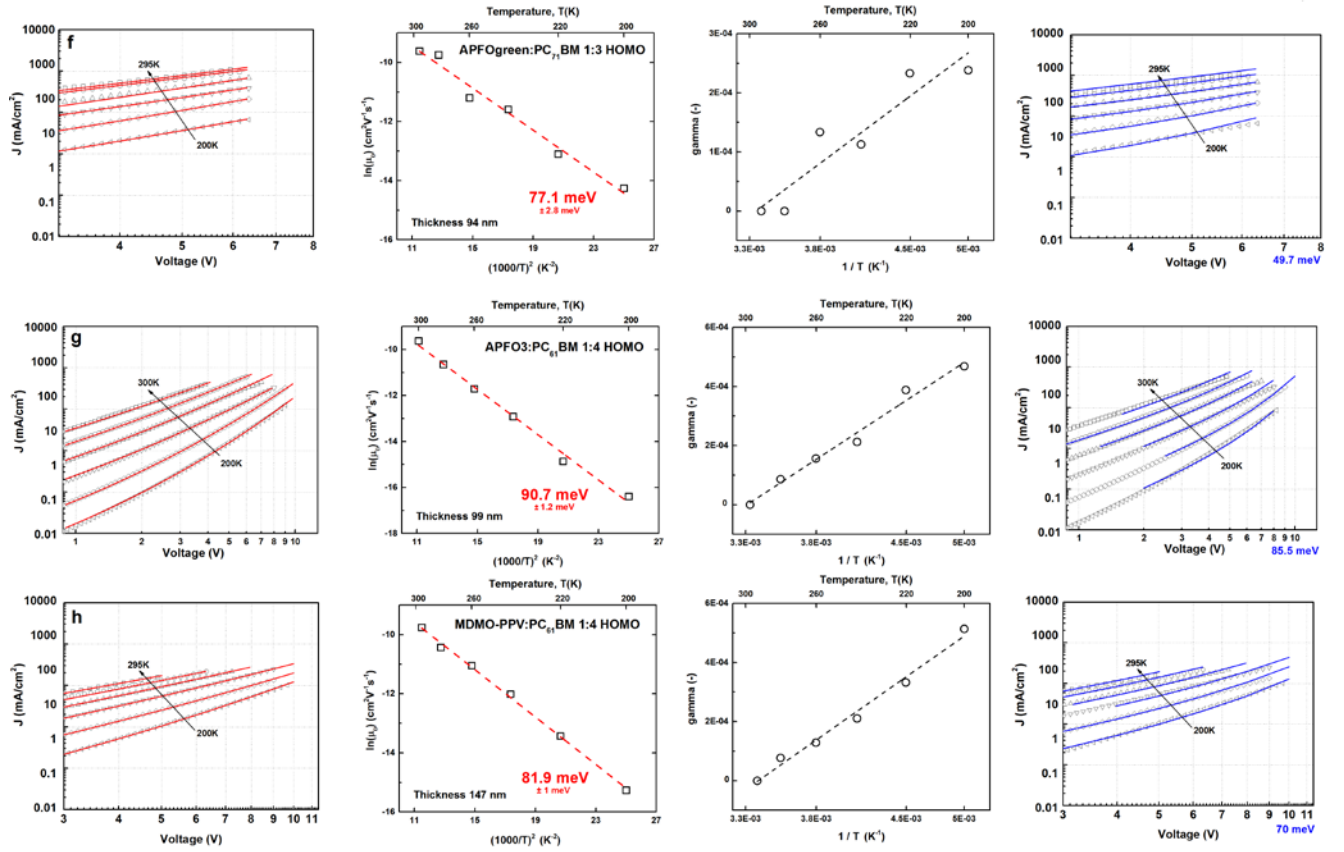
6 - Fitting parameters of DD+eGDM model of Figure 3

	Thickness	ϕ_1	ϕ_2	Hopping rate	Error JV	a_{NN}
	[nm]	[meV]	[meV]	[s⁻¹]	[-]	[nm]
TQ1:PC$_{71}$BM 1:1	110	100	69	$4.22 \cdot 10^9$	0.02	1.75
TQ1:PC$_{71}$BM:IC$_{60}$BA 1:0.7:0.3	115	98	80	$9.33 \cdot 10^9$	0.039	1.71
TQ1:PC$_{71}$BM:IC$_{60}$BA 1:0.5:0.5	120	100	68	$6.15 \cdot 10^9$	0.029	1.93
TQ1:PC$_{71}$BM:IC$_{60}$BA 1:0.3:0.7	110	160	155	$6 \cdot 10^{8*}$	0.093	1.8*
TQ1:IC$_{60}$BA 1:1	110	99	82	$2.66 \cdot 10^9$	0.019	1.76

Table S3. Simulation parameters from the fitting of TQ1:PC$_{71}$BM$_{1-x}$:IC$_{60}$BA$_x$ (0 ≤ x ≤ 1) hole-only devices with the DD+eGDM model in auto-range mode. *This hopping rate and α$_{NN}$ were fixed as the current density of the TQ1:PC$_{71}$BM:IC$_{60}$BA 1:0.3:0.7 hole-only devices was low and resulted in high disorder (~125meV) to balance the relatively high hopping rate of ~$5 \cdot 10^9$.

7

Figure S2. (Left) Hole-only SCLC data fitted with the Murgatroyd-Gill law.[4,5] (Middle-left) Gaussian disorder model fit and active layer thickness. (Middle-right) Linear fit of the gamma values according to equation 17 in the main text. (Right) SCLC data fitted with the Drift Diffusion model.

8 - Gaussian disorder and room temperature zero-field mobilities for MG+GDM and DD+eGDM models of the hole-only devices in Figure 4

	GDM		ODDD	
	σ_{HOMO} [meV]	μ_0 (300 K) [cm²V⁻¹s⁻¹]	σ_{HOMO} [meV]	μ_0 (300 K) [cm²V⁻¹s⁻¹]
PCDTBT pristine	72.2	$1.81 \cdot 10^{-4}$	52.9	$1.01 \cdot 10^{-4}$
TQ1 pristine	94.6	$7.49 \cdot 10^{-6}$	92.7	$5.66 \cdot 10^{-6}$
rrP3HT:PC$_{61}$BM 1:1	62.2	$4.29 \cdot 10^{-5}$	48.1	$2.46 \cdot 10^{-5}$
TQ1:PC$_{71}$BM 1:1	86.8	$6.62 \cdot 10^{-6}$	92.2	$6.71 \cdot 10^{-6}$
TQ1:IC$_{60}$BA 1:1	88.1	$8.66 \cdot 10^{-6}$	89.8	$5.76 \cdot 10^{-6}$
PTB7:PC$_{71}$BM 1:1.5	65.3	$2.78 \cdot 10^{-4}$	47.7	$2.86 \cdot 10^{-4}$
TQ1:PC$_{71}$BM 1:2.5	85.9	$3.48 \cdot 10^{-5}$	74.9	$2.27 \cdot 10^{-5}$
APFOGreen:PC$_{71}$BM 1:3	77.1	$6.69 \cdot 10^{-5}$	49.7	$7.93 \cdot 10^{-5}$
APFO3:PC$_{61}$BM 1:4	90.7	$6.59 \cdot 10^{-5}$	85.5	$4.12 \cdot 10^{-5}$
MDMO_PPV:PC$_{61}$BM 1:4	81.9	$5.78 \cdot 10^{-5}$	70	$4.27 \cdot 10^{-5}$

Table S4. Gaussian energetic disorder and room temperature zero-field mobilities from the MG+GDM and DD+eGDM models for pure and binary hole-only devices of Figure 4.

The settings and initial parameter values are the same as in section 4 in the SI.

9

9 - Fitting parameters of MG+GDM model of Figure 3

| | Vbi | μ^* | B | T_0 | Error JV |
	[V]	[m²V⁻¹s⁻¹]	[-]	[K]	[-]
PCDTBT pristine	0.19	$7.32 \cdot 10^{-7}$	$2.11 \cdot 10^{-5}$	268.3	0.0071
TQ1 pristine	-0.199	$2.48 \cdot 10^{-7}$	$3.16 \cdot 10^{-5}$	324.2	0.002
rrP3HT:PC$_{61}$BM 1:1	0.0113	$5.9 \cdot 10^{-8}$	$1.44 \cdot 10^{-5}$	290.3	$2.1 \cdot 10^{-5}$
TQ1:PC$_{71}$BM 1:1	0.0055	$9.85 \cdot 10^{-8}$	$1.9 \cdot 10^{-5}$	379.6	0.00644
TQ1:IC$_{60}$BA 1:1	-0.0320	$1.23 \cdot 10^{-7}$	$2.23 \cdot 10^{-5}$	336.2	0.00213
PTB7:PC$_{71}$BM 1:1.5	-0.199	$5.22 \cdot 10^{-7}$	$1.42 \cdot 10^{-5}$	264.7	$8.7 \cdot 10^{-4}$
TQ1:PC$_{71}$BM 1:2.5	-0.077	$5.35 \cdot 10^{-7}$	$2.5 \cdot 10^{-5}$	283.8	$2.9 \cdot 10^{-4}$
APFOGreen:PC$_{71}$BM 1:3	-0.199	$3.93 \cdot 10^{-7}$	$1.39 \cdot 10^{-5}$	298.6	0.0019
APFO3:PC$_{61}$BM 1:4	-0.19	$1.27 \cdot 10^{-6}$	$2.45 \cdot 10^{-5}$	302.1	0.0012
MDMO_PPV:PC$_{61}$BM 1:4	-0.139	$5.71 \cdot 10^{-7}$	$2.64 \cdot 10^{-5}$	293.9	0.0019

Table S5. Fitting parameters for pristine, binary and ternary hole-only devices of Figure 4 extracted from the MG+GDM model in auto-range mode.

For the material systems TQ1 pristine, PTB7:PC$_{71}$BM 1:1.5, APFOGreen:PC$_{71}$BM 1:3 and APFO3:PC$_{61}$BM 1:4 the V$_{bi}$ was ~0.4V when the fitting margins were set to 'infinity'. However, the improvement on the JV fits and the difference in the mobilities and energetic disorder were negligible.

10 - Fitting parameters of DD+eGDM model of Figure 4

| | Thickness | φ1 | φ2 | Hopping rate | Error JV | a$_{NN}$ |
	[nm]	[meV]	[meV]	[s⁻¹]	[-]	[nm]
PCDTBT pristine	80	168	123	$1.12 \cdot 10^9$	0.001	1.66
TQ1 pristine	160	127	57	$3.12 \cdot 10^9$	0.068	1.93
rrP3HT:PC$_{61}$BM 1:1	78	111	85.7	$2 \cdot 10^8$	0.01	1.59
TQ1:PC$_{71}$BM 1:1	110	100	69	$4.22 \cdot 10^9$	0.02	1.75
TQ1:IC$_{60}$BA 1:1	110	99	82	$2.66 \cdot 10^9$	0.019	1.76
PTB7:PC$_{71}$BM 1:1.5	140	30	148	$2 \cdot 10^9$	0.004	1.3
TQ1:PC$_{71}$BM 1:2.5	80	101	105	$3.37 \cdot 10^9$	0.028	1.31
APFOGreen:PC$_{71}$BM 1:3	94	196	158	$3.58 \cdot 10^8$	0.03	2.28
APFO3:PC$_{61}$BM 1:4	99	134	53.7	$2.06 \cdot 10^{10}$	0.02	1.3
MDMO_PPV:PC$_{61}$BM 1:4	147	103	96.9	$1.8 \cdot 10^9$	0.04	1.9

Table S6. Fitting parameters for pristine, binary and ternary hole-only devices of Figure 4 extracted from the DD+eGDM model in auto-range mode. The simulations were run with the same settings and initial guesses as in section 5.
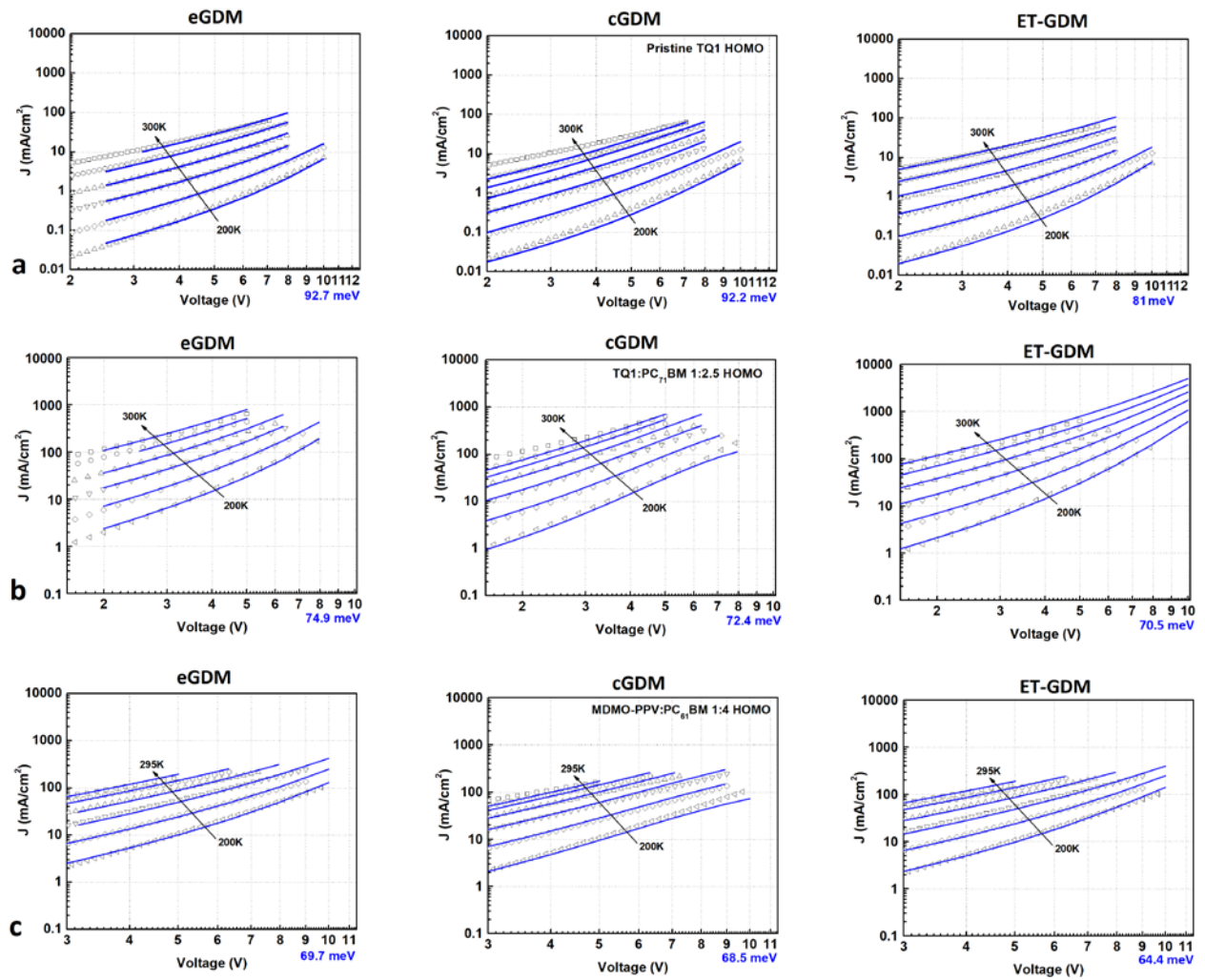
Figure S3. SCLC fits and extracted Gaussian disorder (in blue) for DD+eGDM, cGDM and ET-GDM for a) pristine TQ1 b) TQ1:PC$_{71}$BM 1:2.5 and c) MDMO-PPV:PC$_{61}$BM 1:4

12 – DD+ET-GDM fitting parameters

	v_0 [s^{-1}]	Error JV [-]	a_{NN} [nm]	σ [meV]	α [nm]
PCDTBT pristine	$1.025 \cdot 10^9$	0.028	1.94	61.6	0.22
TQ1 pristine	$1.074 \cdot 10^9$	0.067	1.10	81	0.32
TQ1:PC$_{71}$BM 1:1	$1.1 \cdot 10^9$	0.03	1.18	81.3	0.3
TQ1:PC$_{71}$BM:IC$_{60}$BA 1:0.7:0.3	$1.27 \cdot 10^9$	0.04	1.75	82	0.26
TQ1:PC$_{71}$BM:IC$_{60}$BA 1:0.5:0.5	$1.64 \cdot 10^9$	0.03	1.47	75.2	0.34
TQ1:PC$_{71}$BM:IC$_{60}$BA 1:0.3:0.7	$1.1 \cdot 10^9$	0.129	1.1	89.6	0.31
TQ1:IC$_{60}$BA 1:1	$1 \cdot 10^9$	0.03	1	78.9	0.3
rrP3HT:PC$_{61}$BM 1:1	$1 \cdot 10^9$	0.9	1	57.3*	0.27
PTB7:PC$_{71}$BM 1:1.5	$2.2 \cdot 10^9$	0.002	1.45	53.1	0.13
TQ1:PC$_{71}$BM 1:2.5	$1.02 \cdot 10^9$	0.02	1.26	70.2	0.20
APFOGreen:PC$_{71}$BM 1:3	$2 \cdot 10^9$	0.03	1.36	68.3	0.19
APFO3:PC$_{61}$BM 1:4	$1.7 \cdot 10^9$	0.019	2.05	82.3	0.18
MDMO_PPV:PC$_{61}$BM 1:4	$1.41 \cdot 10^9$	0.04	1.21	64.4	0.33

Table S7. Extracted parameters from fitting the temperature dependent SCLC data with the DD+ET-GDM model for all material systems. *The model could not accurately fit the data for rrP3HT:PC$_{61}$BM 1:1

# 13 - Arrhenius analysis for μ^*=10 cm^{2}V^{-1}s^{-1}
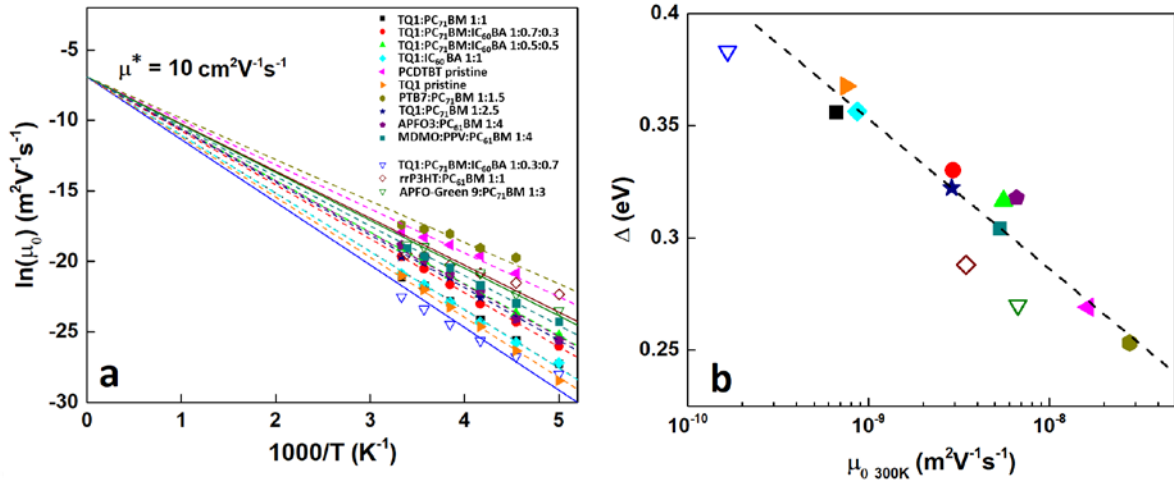
Figure S4. a) Zero-field mobilities for hole-only pristine, binary and ternary material systems fitted with equation 17 in the main text with Δ as a free parameter and a fixed μ^*=10 cm^{2}V^{-1}s^{-1}. The plot is scaled as in Ref. [7] showing a 'universal' μ^* at infinite temperature. Open symbols with solid line fits indicate the material systems that do not show strong correlation between Δ and zero field mobility at 300 K b) Resulting Δ values versus zero field mobilities at 300 K for all material systems investigated in this work. The dashed line is a guide to the eye. Stronger correlation (10 out of 13 material systems, indicated with solid symbols) is noticed when μ^* is set equal to 10 cm^{2}V^{-1}s^{-1} compared to μ^* set as a free parameter (c.f. Figure 5 and discussion in the main text).
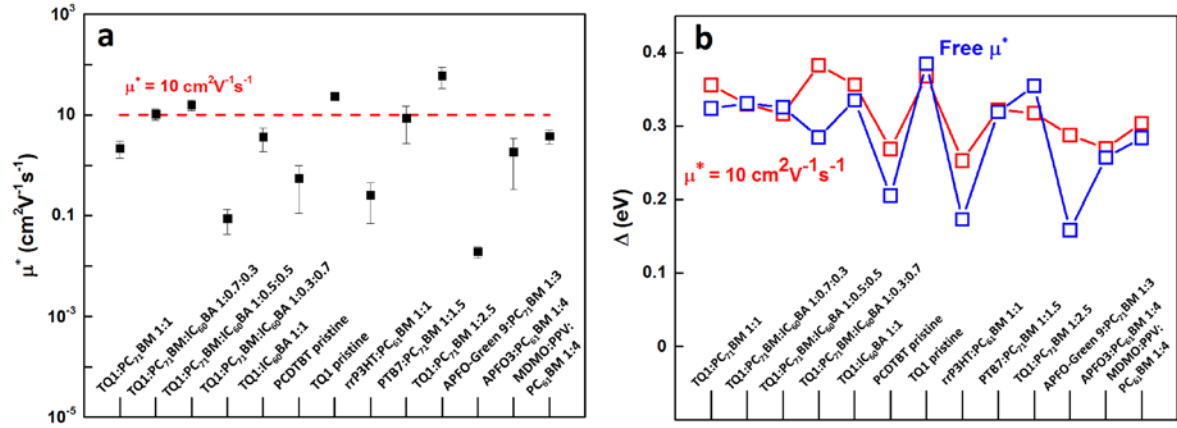
Figure S5. a) Zero-field mobilities at infinite temperature for hole-only pristine, binary and ternary material systems fitted with equation 17 in the main text with μ^* and Δ set as free parameters (black squares). The red dashed line is the fixed $\mu^*=10$ cm^{2}V^{-1}s^{-1}. b) Activation energies Δ for free μ^*(blue traces) and fixed $\mu^*=10$ cm^{2}V^{-1}s^{-1} (red traces).

|	Free μ^* [cm^{2}V^{-1}s^{-1}]	Δ [eV]	Δ $\mu^*=10$ cm^{2}V^{-1}s^{-1} [meV]
TQ1:PC$_{71}$BM 1:1	2.18	0.32	0.35
TQ1:PC$_{71}$BM:IC$_{60}$BA 1:0.7:0.3	10.49	0.33	0.33
TQ1:PC$_{71}$BM:IC$_{60}$BA 1:0.5:0.5	15.75	0.32	0.31
TQ1:PC$_{71}$BM:IC$_{60}$BA 1:0.3:0.7	0.08	0.28	0.38
TQ1:IC$_{60}$BA 1:1	3.66	0.33	0.35
PCDTBT pristine	0.54	0.20	0.26
TQ1 pristine	23.34	0.38	0.36
rrP3HT:PC$_{61}$BM 1:1	0.019	0.15	0.28
PTB7:PC$_{71}$BM 1:1.5	0.25	0.17	0.25
TQ1:PC$_{71}$BM 1:2.5	8.76	0.31	0.32
APFOGreen:PC$_{71}$BM 1:3	1.86	0.25	0.26
APFO3:PC$_{61}$BM 1:4	60.16	0.35	0.31
MDMO_PPV:PC$_{61}$BM 1:4	3.82	0.28	0.3

Table S8. Fitting parameters from Arrhenius-type analysis of all material systems with equation 17 in the main text for free and constrained μ^*(show in Figures S3,S4).
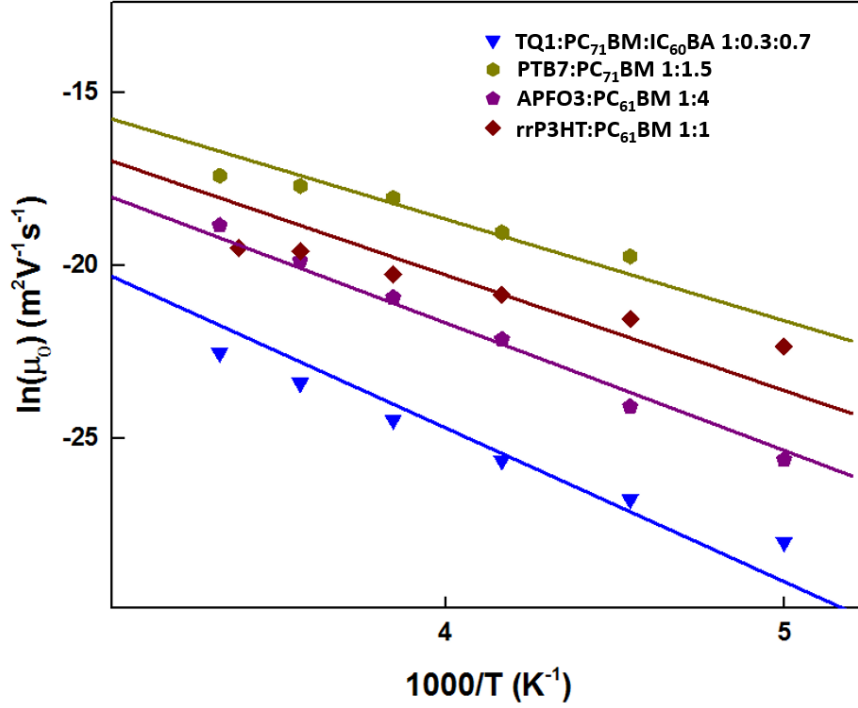
Figure S6. Zoomed-in view of zero-field mobilities for hole-only devices fitted with equation 17 using a fixed $\mu^* = 10$ cm^{2}V^{-1}s^{-1} while the activation energy Δ is set as a free fitting parameter. The universal μ^* does not result in good fits for TQ1:PC$_{71}$BM:IC$_{60}$BA 1:0.3:0.7, PTB7:PC$_{71}$BM 1:1.5, APFO3:PC$_{61}$BM 1:4 and rrP3HT:PC$_{61}$BM 1:1 hole-only devices.

14 - Forced γ=0 mobility and disorder analysis for APFO3:PC$_{61}$BM 1:4
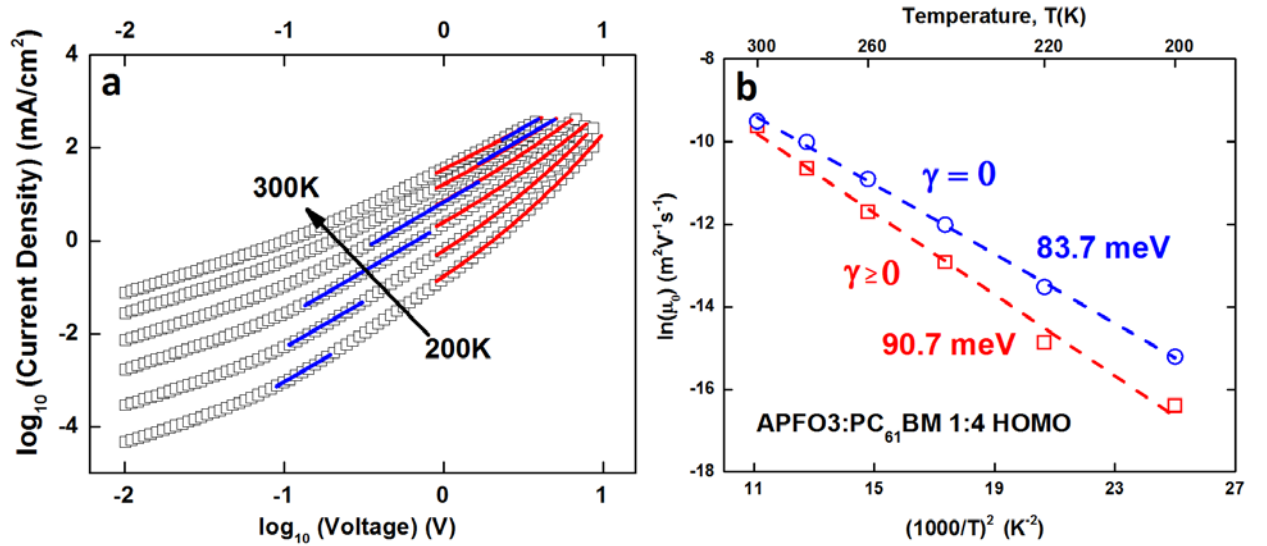
Figure S7. a) Temperature-dependent SCLC data for APFO3:PC$_{61}$BM 1:4 hole-only devices (black open symbols) fitted with Eq. 17 using γ ≥ 0 (red lines) and γ = 0 (blue lines); b) Extracted zero-field mobilities vs 1/T^2 for γ ≥ 0 (red open squares) and γ = 0 (blue open circles).

15 - Material Abbreviations

TQ1 = poly[[2,3-bis(3-octyloxyphenyl)-5,8-quinoxalinediyl]-2,5-thiophenediyl]

$PC_{71}BM$ = [6,6]-phenyl C71 butyric acid methyl ester

$PC_{61}BM$ = [6,6]-phenyl C61 butyric acid methyl ester

$IC_{60}BA$ = 1',1'',4',4''-tetrahydro-di[1,4]methanonaphthaleno-[1,2:2',3',56,60:2',3''][5,6]fullerene-C60

PTB7 = poly({4,8-bis[(2-ethylhexyl)oxy]benzo[1,2-b:4,5-b']-dithiophene-2,6-diyl}{3-fluoro-2-[(2-ethylhexyl)carbonyl]-thieno[3,4-b]thiophenediyl})

P3HT = poly(3-hexylthiophene-2,5-diyl)

PCDTBT = poly[N-9'-heptadecanyl-2,7-carbazole-alt-5,5-(4',7'-di-2-thienyl-2',1',3'-benzothiadiazole)], poly[[9-(1-octylnonyl)-9H-carbazole-2,7-diyl]-2,5-thiophenediyl-2,1,3-benzothiadiazole-4,7-diyl-2,5-thiophenediyl]

MDMO PPV = poly[2-methoxy-5-(3',7'-dimethyloctyloxy)-1,4-phenylenevinylene]

APFO3 = poly[(9,9-dioctylfluorenyl-2,7-diyl)-alt-5,5-(40,70-di-2-thienyl-20,10,30-benzothiadiazole)]

16 – Fabrication parameters

	c [g/L]	solvent	Spin coating speed [rpm / sec]
PCDTBT pristine	25	ODCB	500 / 120
TQ1 pristine	25	ODCB	500 / 60
TQ1:$PC_{71}BM$ 1:1	25	ODCB	500 / 60
TQ1:$PC_{71}BM$:$IC_{60}BA$ 1:0.7:0.3	25	ODCB	500 / 60
TQ1:$PC_{71}BM$:$IC_{60}BA$ 1:0.5:0.5	25	ODCB	500 / 60
TQ1:$PC_{71}BM$:$IC_{60}BA$ 1:0.3:0.7	25	ODCB	500 / 60
TQ1:$IC_{60}BA$ 1:1	25	ODCB	500 / 60
rrP3HT:$PC_{61}BM$ 1:1	20	CB	1000 / 60
PTB7:$PC_{71}BM$ 1:1.5	20	ODCB	500 / 60
TQ1:$PC_{71}BM$ 1:2.5	25	ODCB	500 / 60
APFOGreen:$PC_{71}BM$ 1:3	15	CF	1500 / 60
APFO3:$PC_{61}BM$ 1:4	20	CF	1500 / 60
MDMO_PPV:$PC_{61}BM$ 1:4	20	CB	500 / 60

Table S9. Solvent, active layer concentration and spin coating speed parameters for all material systems

None of the material systems was annealed or blended with any additives. After the first spin coating step (indicated in the table) all samples were dried with a second spin coating step of 3000 rpm for 60 seconds.

17 - References

[1] D.L. Scharfetter, H.K. Gummel, Large-signal analysis of a silicon Read diode oscillator, IEEE Trans. Electron Devices. 16 (1969) 64–77. doi:10.1109/T-ED.1969.16566.

[2] C. Pflumm, Simulation homogener Barrierenentladungen inklusive der Elektrodenbereiche, Tenea, 2004.

[3] W.R. Frensley, Scharfetter-Gummel Discretization Scheme for Drift-Diffusion Equations, Numer. Simul. Optoelectron. Devices NUSOD. (2004). doi:10.1109/NUSOD.2012.6316560.

[4] P.N. Murgatroyd, Theory of space-charge-limited current enhanced by Frenkel effect, J. Phys. Appl. Phys. 3 (1970) 308. doi:10.1088/0022-3727/3/2/308.

[5] W.D. Gill, Drift mobilities in amorphous charge-transfer complexes of trinitrofluorenone and poly-n-vinylcarbazole, J. Appl. Phys. 43 (1972) 5033–5040. doi:10.1063/1.1661065.

[6] N. Felekidis, A. Melianas, M. Kemerink, Design Rule for Improved Open-Circuit Voltage in Binary and Ternary Organic Solar Cells, ACS Appl. Mater. Interfaces. 9 (2017). doi:10.1021/acsami.7b08276.

[7] N.I. Craciun, J. Wildeman, P.W.M. Blom, Universal Arrhenius Temperature Activated Charge Transport in Diodes from Disordered Organic Semiconductors, (n.d.). doi:10.1103/PhysRevLett.100.056601.